

# Making Higher Order MOT Scalable: An Efficient Approximate Solver for Lifted Disjoint Paths

Andrea Hornakova<sup>\*1</sup>    Timo Kaiser<sup>\*2</sup>    Paul Swoboda<sup>1</sup>    Michal Rolinek<sup>3</sup>  
 Bodo Rosenhahn<sup>2</sup>    Roberto Henschel<sup>2</sup>

<sup>\*</sup>Authors contributed equally, <sup>1</sup>Max Planck Institute for Informatics, Saarland Informatics Campus, <sup>2</sup>Institute for Information Processing, Leibniz University Hannover, <sup>3</sup>Max Planck Institute for Intelligent Systems, Tübingen

## Abstract

We present an efficient approximate message passing solver for the lifted disjoint paths problem (LDP), a natural but NP-hard model for multiple object tracking (MOT). Our tracker scales to very large instances that come from long and crowded MOT sequences. Our approximate solver enables us to process the MOT15/16/17 benchmarks without sacrificing solution quality and allows for solving MOT20, which has been out of reach up to now for LDP solvers due to its size and complexity. On all these four standard MOT benchmarks we achieve performance comparable or better than current state-of-the-art methods including a tracker based on an optimal LDP solver.

## 1. Introduction

Deriving high-level understanding from a video is a desired task that has been studied in computer vision for a long time. Nevertheless, solving the problem is a long way off. A computer vision system able to extract the motions of objects appearing in a video in terms of trajectories is considered as a prerequisite for the goal. This task, called multiple object tracking (MOT), has numerous applications, e.g. in the area of video surveillance [18], sports analysis [2, 42], urban planning [3], or autonomous driving [39, 19].

Yet, solving MOT is challenging, especially for long and crowded sequences. The predominant approach for MOT is the tracking-by-detection paradigm, which splits the problem into two subtasks. First, objects are detected in all video frames by an object detector. Then, the detections are linked across frames to form trajectories. While the performance of object detectors has improved considerably by recent advances of CNNs [47, 63, 46, 17], the latter task called the *data association* remains challenging. The data association reasons from *pairwise costs*, which indicate for each pair of detections the likelihood of belonging to the same object.

Appearance and spatio-temporal information are often

ambiguous, especially in crowded scenes and pairwise costs can be misleading. Moreover, object detectors produce more errors in crowded scenes due to partial occlusions. To resolve these issues, it is crucial that the data association incorporates global context.

The disjoint paths problem (DP) [65, 35] is a natural model for MOT. Results are computed efficiently using a min-cost flow algorithm that delivers the global optimal solution. Unfortunately, the integration of long range temporal interactions is limited, as DP obeys the first-order Markov-chain assumption: for each trajectory, consistency is ensured only between directly linked detections, which is a strong simplification that ignores higher order consistencies among multiple linked detections.

To fix this deficiency, [28] generalizes DP to lifted disjoint paths (LDP) by using additional connectivity priors in terms of *lifted edges*. This makes the formulation much more expressive while it maintains the feasibility set of the DP (Sec. 3). The optimization problem enables to take into account pairwise costs between arbitrary detections belonging to one trajectory. It thus enables to incorporate long range temporal interactions effectively and leads to considerable improvement of recall and precision [28]. Similar extensions have been made for the multicut problem [56, 57].

While the integration of the global context by LDP is crucial to obtain high-quality tracking results, it makes the data association problem NP-hard. Still, [28] presented a global optimal LDP solver usable for semi-crowded sequences with reasonable computational effort. However, when applied to longer and crowded sequences, such approaches are not tractable anymore, due to too high demands on runtime and memory.

In order to close this gap, we present the first approximate solver for LDP. The resulting tracker scales to big problem instances and incorporates global context with similar accuracy as the global optimal LDP solver. Moreover, our solver outputs certificates in terms of primal/dual gaps.

In particular, our solver is based on a Lagrangean (dual) decomposition of the problem. This dual is iteratively opti-

mized by dual block coordinate ascent (a.k.a. message passing) using techniques from [54], see Sec. 4.1. The decomposition relies on subproblems that are added in a cutting plane fashion. We obtain high-quality primal solutions by solving minimum cost flow problems with edge costs synthesizing information from both base and lifted edges from the dual task and improve them via a local search procedure.

We validate the quality of the solver on four standard MOT benchmarks (Sec. 5). We achieve comparable or better performance w.r.t. the current state-of-the-art trackers including the tracker based on the optimal LDP solver [28] on MOT15/16/17 [37, 45]. Furthermore, our proposed tracker performs on par with state-of-the-art on the more challenging MOT20 dataset [16] which is composed of long and crowded sequences. Lightweight features and a fast solver are crucial to perform tracking on such massive sequences. Our work thus extends the applicability of the successful LDP formulation to a wider range of instances.

**Contribution** of this work is in summary as follows:

- We make the LDP problem more accessible and applicable by introducing an approximate solver with better scalability properties than the global optimal LDP solver, while resulting in similar tracking performance, and being independent of Gurobi [22].
- We present an MOT system that is scalable to challenging sequences by using considerably less computationally demanding features than what is used in the state-of-the-art tracker [28]. Our system incorporates higher order consistencies in a scalable way, i.e. it uses an approximate solver and provides a gap to the optimum.

We make our LDP solver<sup>1</sup> and our MOT pipeline<sup>2</sup> available.

## 2. Related Work

**(Lifted) disjoint paths.** The disjoint paths problem is a natural model for multiple object tracking and is solvable with fast combinatorial solvers [35]. It has been used for the data association step of MOT in [6, 65]. Its extensions have been used for fusing different object detectors [12] or multi-camera MOT [27, 38]. Its main disadvantage is that it does not allow to integrate long range information because it evaluates only direct connections between object detections within a trajectory. The lifted disjoint paths problem introduced in [28] enhances DP by introducing lifted edges that enable to reward or penalize arbitrary connections between object detections. This incorporation of long range information leads to a significant improvement of the tracking performance yielding state-of-the-art results on main MOT benchmark but makes the problem NP-hard. The authors provide a globally optimal solver using Gurobi [22]. Despite a lot of efficient subroutines, the general time com-

plexity of the provided solver remains exponential. Therefore, in order to extend LDP-based methods to highly dense MOT problems as in MOT20 it is crucial to reduce the complexity of the used LDP solver because the number of feasible connections between detections increases dramatically.

**Multicut and lifted multicut.** LDP is similar to (lifted) multicut [14, 29]. Multicut has been used for MOT in [26, 33, 36, 51, 55, 56], lifted multicut in [5, 57]. These trackers solve the underlying combinatorial problem approximately via heuristics without providing an estimation of the gap to optimality. Our approach, delivers an approximate solution together with a lower bound enabling to assess the quality of the solution. Additionally, LDP provides a strictly better relaxation than lifted multicut [28].

**Other data association models for MOT.** Several works employ greedy heuristics to obtain tracking results [9, 68, 7]. Such strategies normally suffer from occlusions or ambiguous situations, causing trajectory errors. Others use bipartite matchings [31, 52, 69, 62, 61, 60] to assign new detections with already computed trajectories of the past optimally. Since no global context is incorporated, they are prone to errors if individual edge costs are misleading.

Higher order MOT frameworks ensure consistencies within all detections of a trajectory. This can be done greedily, by computing one trajectory at a time via a generalized minimum clique problem [64], or globally using an extension to the maximum multi clique problem [15].

Several works employ continuous domain relaxation. When MOT is formulated as a binary quadratic program [23, 25, 58, 24], a modification of the Frank-Wolfe algorithm adapted to the non-convex case has been used [23]. Some approximations for binary linear programs use an LP-relaxation, optimize in the continuous domain and derive a binary solution from the continuous one [32, 12, 11]. They however do not provide the optimality gap, in contrast to our work. Higher order MOT can be considered as a classification problem using graph convolutions [10]. It allows to train features directly on the tracking task.

The multigraph-matching problem, a generalization of the graph matching problem, has been used for MOT [30]. Here, cycle consistency constraints of the multi-graph matching ensures higher order consistencies of the trajectories. Message passing for higher order matching in MOT has been used in [4] employing a variant of MPLP [20]. In contrast to our formulation, [4] does not model occlusions and does not allow for connectivity priors.

Probabilistic approaches to multiple-target tracking include multiple hypotheses tracking [34, 13], joint probabilistic data association [48, 53] and others [53, 44].

## 3. Problem Formulation

The lifted disjoint paths problem (LDP) introduced in [28] is an optimization problem for finding a set of

<sup>1</sup><https://github.com/LPMP/LPMP>

<sup>2</sup><https://github.com/TimoK93/ApLift>

vertex-disjoint paths in a directed acyclic graph. The cost of each path is determined by the cost of edges in that path as in the basic disjoint paths problem (DP), but additionally there are higher order costs defined by lifted edges. A lifted edge contributes to the cost if its endpoints are part of the same path. This problem is a natural formulation for multiple object tracking (MOT), where lifted edges allow to reidentify the same objects over long distance.

While of greater expressivity, the LDP is NP-hard [28] in contrast to DP which is reducible to the minimum cost flow. Below, we recapitulate the formulation of LDP from [28].

### 3.1. Notation and Definitions.

**Flow network:** a directed acyclic graph  $G = (V, E)$ .

**Start and terminal:** nodes  $s, t \in V$ .

**Lifted graph:** a directed acyclic graph  $G' = (V', E')$ , where  $V' = V \setminus \{s, t\}$ .

**The set of paths** starting at  $v$  and ending in  $w$  is

$$vw\text{-paths}(G) = \left\{ (v_1 v_2, \dots, v_{l-1} v_l) : \begin{array}{l} v_i v_{i+1} \in E, \\ v_1 = v, v_l = w \end{array} \right\}. \quad (1)$$

For a  $vw$ -path  $P$  its edge set is  $P_E$  and its node set is  $P_V$ .

**Reachability relation** for two nodes  $v, w \in V$  is defined as  $vw \in \mathcal{R}_G \Leftrightarrow vw\text{-paths}(G) \neq \emptyset$ . We assume that it is reflexive and  $su \in \mathcal{R}_G, ut \in \mathcal{R}_G \forall u \in V$ , i.e. all nodes can be reached from  $s$  and all nodes can reach the sink node  $t$ .

**Flow variables:** Variables  $y \in \{0, 1\}^E$  have value 1 if flow passes through the respective edges.

**Node variables**  $z \in \{0, 1\}^V$  denote flow passing through each node. Values 0/1 forces paths to be node-disjoint.

**Variables of the lifted edges**  $E'$  are denoted by  $y' \in \{0, 1\}^{E'}$ .  $y'_{vw} = 1$  signifies that nodes  $v$  and  $w$  are connected via the flow  $y$  in  $G$ . Formally,

$$y'_{vw} = 1 \Leftrightarrow \exists P \in vw\text{-paths}(G) : \forall ij \in P_E : y_{ij} = 1. \quad (2)$$

**Lifted disjoint paths problem.** Given edge costs  $c \in \mathbb{R}^E$ , node cost  $d \in \mathbb{R}^V$  in flow network  $G$  and edge cost  $c' \in \mathbb{R}^{E'}$  for the lifted graph  $G'$  the lifted disjoint paths problem is

$$\begin{aligned} \min_{\substack{y \in \{0,1\}^E, y' \in \{0,1\}^{E'}, \\ z \in \{0,1\}^V}} & \langle c, y \rangle + \langle c', y' \rangle + \langle d, z \rangle \\ \text{s.t.} & \quad y \text{ node-disjoint } s, t\text{-flow in } G, \\ & \quad z \text{ flow through nodes of } G \\ & \quad y, y' \text{ feasible according to (2)} \end{aligned} \quad (3)$$

Set  $E'$  can be arbitrary. It makes sense to create a lifted edge  $vw$  only if  $vw \in \mathcal{R}_G$  due to Formula (2) and only if  $v$  and  $w$  do not belong to neighboring frames. We describe our choice in Sec. 5.2.

Other notation and abbreviations are in Appendix 8.1.

## 4. Lagrange Decomposition Algorithm for LDP

Below we recapitulate Lagrange decomposition and the message passing primitive used in our algorithm (Sec. 4.1). Then, we propose a decomposition of the LDP problem (3) into smaller but tractable subproblems (Sec. 4.2-4.4). This decomposition is a dual task to an LP-relaxation of (3). Therefore, it provides a lower bound that is iteratively increased by the message passing. We solve Problem (3) in a simplified version of Lagrange decomposition framework developed in [54]. Our heuristic for obtaining primal solutions uses the dual costs from the subproblems (Sec. 4.6).

### 4.1. Lagrange Decomposition

We have an optimization problem  $\min_{x \in \mathcal{X}} \langle c, x \rangle$  where  $\mathcal{X} \subseteq \{0, 1\}^n$  is a feasible set and  $c \in \mathbb{R}^n$  is the objective vector. Its Lagrange decomposition is given by a set of subproblems  $\mathcal{S}$  with associated feasible sets  $\mathcal{X}^s \subseteq \{0, 1\}^{d_s}$  for each  $s \in \mathcal{S}$ . Each coordinate  $i$  of  $\mathcal{X}^s$  corresponds to one coordinate of  $\mathcal{X}$  via an injection  $\pi_s : [d_s] \rightarrow [n]$  alternatively represented by a matrix  $A^s \in \{0, 1\}^{d_s \times n}$  where  $(A^s)_{ij} = 1 \Leftrightarrow \pi_s(i) = j$ . For each pair of subproblems  $s, s' \in \mathcal{S}$  that contain a pair of coordinates  $i, j$  such that  $\pi_s(i) = \pi_{s'}(j)$ , we have a coupling constraint  $x_i^s = x_j^{s'}$  for each  $x^s \in \mathcal{X}^s, x^{s'} \in \mathcal{X}^{s'}$ .

We require that every feasible solution  $x \in \mathcal{X}$  is feasible for the subproblems, i.e.  $\forall x \in \mathcal{X}, \forall s \in \mathcal{S} : A^s x \in \mathcal{X}^s$ .

We require that the objectives of subproblems are equivalent to the original objective, i.e.  $\langle c, x \rangle = \sum_{s \in \mathcal{S}} \langle \theta^s, A^s x \rangle \forall x \in \mathcal{X}$ . Here,  $\theta^s \in \mathbb{R}^{d_s}$  defines the objective of subproblem  $s$ .

The lower bound of the Lagrange decomposition given the costs  $\theta^s$  for each  $s \in \mathcal{S}$  is

$$\sum_{s \in \mathcal{S}} \min_{x^s \in \mathcal{X}^s} \langle \theta^s, x^s \rangle. \quad (4)$$

Given coupling constraint  $x_i^s = x_j^{s'}$  and  $\gamma \in \mathbb{R}$ , a sequence of operations of the form  $\theta_i^s += \gamma, \theta_j^{s'} -= \gamma$  is called a reparametrization.

Feasible primal solutions are invariant under reparametrizations but the lower bound (4) is not. The optimum of the dual lower bound equals to the optimum of a convex relaxation of the original problem, see [21].

**Min-marginal message passing.** Below, we describe reparametrization updates monotonically non-decreasing in the lower bound based on *min-marginals*. Given a variable  $x_i^s$  of a subproblem  $s \in \mathcal{S}$ , the associated *min-marginal* is

$$m_i^s = \min_{x^s \in \mathcal{X}^s: x_i^s = 1} \langle \theta^s, x^s \rangle - \min_{x^s \in \mathcal{X}^s: x_i^s = 0} \langle \theta^s, x^s \rangle \quad (5)$$

i.e. the difference between the optimal solutions with the chosen variable set to 1 resp. 0.

**Proposition 1** ([54]). *Given a coupling constraints  $x_i^s = x_j^s$  and  $\omega \in [0, 1]$  the following operation is non-decreasing w.r.t. the dual lower bound (4)*

$$\theta_i^s \leftarrow \omega \cdot m_i^s, \quad \theta_j^s \leftarrow \omega \cdot m_i^s. \quad (6)$$

**The goal of reparametrization** is two-fold. (i) Improving the objective lower bound to know how far our solution is from the optimum. (ii) Using reparametrized costs as the input for our primal heuristic yields high-quality primal solutions. The key components are efficient computations of (i) optima of subproblems for obtaining lower bound (4), (ii) constrained optima for obtaining min-marginals (5) and (iii) a primal heuristic using the reparametrized costs (Sec. 4.6). Lagrange decomposition has been used for other problems but the subproblem decomposition and minimization procedures are problem specific. Therefore, developing them for LDP is an important contribution for solving LDP in a scalable way while keeping a small gap to an optimum.

## 4.2. Inflow and Outflow Subproblems

For each node  $v \in V$  of the flow graph, we introduce two subproblems: An inflow and an outflow subproblem. The subproblems contain all incoming resp. outgoing edges of node  $v$  together with the corresponding node. Formally, inflow resp. outflow subproblems contain the edges  $\delta_{E'}^-(v) \cup \delta_{E'}^+(v)$ , resp.  $\delta_E^-(v) \cup \delta_E^+(v)$ . Here, we adopt the standard notation where  $\delta_{E'}^-(v)$ , resp.  $\delta_E^-(v)$  denote all base edges incoming to  $v$ , resp. outgoing from  $v$ . Similarly,  $\delta_{E'}^+(v)$ ,  $\delta_E^+(v)$  denote lifted edges incoming to, resp. outgoing from  $v$ .

**The feasible set**  $\mathcal{X}_v^{out}$  of the outflow subproblem for node  $v$  is defined as

$$\left\{ \begin{array}{l} z_v^{out} \in \{0, 1\}, y^{out} \in \{0, 1\}^{\delta_E^+(v)}, y'^{out} \in \{0, 1\}^{\delta_{E'}^+(v)} : \\ (z_v^{out}, y^{out}, y'^{out}) = \mathbb{0} \vee \\ \exists P \in vt\text{-paths}(G) \text{ s.t.} \quad \begin{array}{l} z_v^{out} = 1 \\ y_{vw}^{out} = 1 \Leftrightarrow vw \in P_E \\ y_{vu}^{out} = 1 \Leftrightarrow u \in P_V \end{array} \end{array} \right\}. \quad (7)$$

Consequently, either there is no flow going through vertex  $v$  and all base and lifted edges have label zero. Alternatively, there exists a  $vt$ -path  $P$  in  $G$  labeled by one. In this case the base edge adjacent to  $v$  corresponding to the first edge in  $P$  is one. All lifted edges connecting  $v$  with vertices of  $P$  also have value one. All other base and lifted edges are zero. Each feasible solution of the outflow subproblem can be represented by a path  $vt$ -path  $P$ . The feasible set of the inflow subproblem  $\mathcal{X}_v^{in}$  is defined analogously. We sometimes omit the superscripts *out* for better readability.

**Constraints between inflow and outflow subproblems.**

For node variables, we add the constraint  $z_v^{in} = z_v^{out}$ . For an edge  $vw \in E \cup E'$  we require the shared edge in the outflow subproblem of  $v$  and in the inflow subproblem for

$w$  to agree, i.e.  $y_{vw}^{out} = y_{vw}^{in}$  if  $vw \in E$  and  $y'_{vw}^{out} = y'_{vw}^{in}$  if  $vw \in E'$ .

**Optimization of in- and outflow subproblems.** Given costs  $\theta^{out}$ , the optimal solution of an outflow problem for node  $v$  can be computed by depth-first search on the subgraph defined by the vertices reachable from  $v$ .

The algorithms rely on the following data structures:

- `lifted_costs[u]` contains the minimum cost of all  $ut$ -paths w.r.t. to costs of all lifted edges connecting  $v$  with the vertices of the path.
- `next[u]` contains the best neighbor of vertex  $u$  w.r.t. values in `lifted_cost`. That is,  $\text{next}[u] = \text{argmin}_{w:uw \in \delta_E^+(u)} \text{lifted\_cost}[w]$

---

### Algorithm 1 Opt-Out-Cost

---

**Input** start vertex  $v$ , edge costs  $\tilde{\theta}$

**Output** optimal value `opt`, `lifted_cost`  $\forall w : vw \in \delta_E^+(v)$   
optimal solution for  $vw$  active  $\alpha_{vw}$

- 1: **for**  $u \in V : vu \in \mathcal{R}_G$  **do**
  - 2:   `lifted_cost[u] =  $\infty$ , next[u] =  $\emptyset$`
  - 3: **end for**
  - 4: `lifted_cost[t] = 0, next[t] = t`
  - 5: `Lifted-Cost-DFS-Out( $v, v, \tilde{\theta}, \text{lifted\_cost}, \text{next}$ )`
  - 6:  $\forall w : vw \in \delta_E^+(v) : \alpha_{vw} = \tilde{\theta}_v + \tilde{\theta}_{vw} + \text{lifted\_cost}[w]$
  - 7: `opt =  $\min(\min_{vw \in \delta_E^+(v)} \alpha_{vw}, 0)$`
- 

---

### Algorithm 2 Lifted-Cost-DFS-Out

---

**Input**  $v, u, \tilde{\theta}$ , `lifted_cost`, `next`

**Output** `lifted_cost`, `next`

- 1:  $\alpha = 0$
  - 2: **for**  $uw \in \delta_E^+(u)$  **do**
  - 3:   **if** `next[w] =  $\emptyset$`  **then** `Lifted-Cost-DFS-Out( $v, w, \tilde{\theta}$ )`
  - 4:   **if** `lifted_cost[w] <  $\alpha$`  **then**
  - 5:      $\alpha = \text{lifted\_cost}[w], \text{next}[u] = w$
  - 6:   **end if**
  - 7: **end for**
  - 8: **if** `next[u] =  $\emptyset$`  **then** `next[u] = t`
  - 9: `lifted_cost[u] =  $\alpha + \tilde{\theta}'_{vu}$`
- 

Alg. 1 and 2 give a general depth first search (DFS) procedure that, given a vertex  $v$ , computes optimal paths from all vertices reachable from  $v$ . Alg. 1 takes as input vertex  $v$  and edge costs  $\tilde{\theta}$ . Its subroutine Alg. 2 computes recursively for each vertex  $u$  reachable from  $v$  the value `lifted_cost[u]`. The overall optimal cost  $\min_{(z,y,y') \in \mathcal{X}_v^{out}} \langle \tilde{\theta}, (z, y, y') \rangle$  of the subproblem is given by the minimum of node and base edge and lifted edges costs  $\min_{vu \in \delta_E^+(v)} \tilde{\theta}_v^{out} + \tilde{\theta}_{vu}^{out} + \text{lifted\_cost}[u]$ . We achieve linear complexity by exploiting that subpaths of minimum cost paths are minimal as well. The optimization for the inflow subproblem is analogous.

**Message passing for in- and outflow subproblems.** We

could compute one min-marginal (5) by adapting Alg. 1 and forcing an edge to be taken or not. However, computing min-marginals one-by-one with performing operation (6) would be inefficient, since it would involve calling Alg. 1  $\mathcal{O}(|\delta_E^+(v)| + |\delta_{E'}^+(v)|)$  times. Therefore, we present efficient algorithms for computing a sequence of min-marginals in Appendix 8.2. The procedures save computations by choosing the order of edges for computing min-marginals suitably and reuse previous calculations.

### 4.3. Path Subproblems

The subproblem contains a lifted edge  $vw$  and a path  $P$  from  $v$  to  $w$  consisting of both base and lifted edges. They reflect that (i) lifted edge  $vw$  must be labelled 1 if there exists an active path between  $v$  and  $w$ , and (ii) there cannot be exactly one inactive lifted edge within path  $P$  if  $vw$  is active. The reason is that the inactive lifted edge divides  $P$  into two segments that must be disconnected. This is contradictory to activating lifted edge  $vw$  because it indicates a connection between  $v$  and  $w$ . Path subproblems are similar to cycle inequalities for the multicut [14].

In order to distinguish between base and lifted edges of path  $P$ , we use notation  $P_E = P \cap E$  and  $P_{E'} = P \cap E'$ . For the purpose of defining the feasible solutions of path subproblems, we define strong base edges  $E_0 = \{vw \in E \mid vw\text{-paths}(G) = \{vw\}\}$ . That is, base edge  $vw$  is strong iff there exists no other  $vw$ -path in graph  $G$  than  $vw$  itself.

**The feasible set**  $\mathcal{X}^P$  of the path subproblem for  $vw$ -path  $P$  is defined as

$$y \in \{0, 1\}^{P_E}, y' \in \{0, 1\}^{P_{E'} \cup \{vw\}} : \quad \forall kl \in P_{E'} \cup \{vw\} : \quad (8)$$

$$\sum_{ij \in P_E} (1 - y_{ij}) + \sum_{ij \in P_{E'} \cup \{vw\} \setminus \{kl\}} (1 - y'_{ij}) \geq 1 - y'_{kl},$$

$$\forall kl \in P_E \cap E_0 : \quad (9)$$

$$\sum_{ij \in P_E \setminus kl} (1 - y_{ij}) + \sum_{ij \in P_{E'} \cup \{vw\}} (1 - y_{ij}) \geq 1 - y_{kl}.$$

Equation (8) requires that a lifted edge in  $P_{E'}$  or  $vw$  can be zero only if at least one other edge of the subproblem is zero. Equation (9) enforces the same for strong base edges.

**The optimization of path subproblems** is detailed in Alg. 12 in the Appendix. The principle is as follows. It checks whether there exists exactly one positive edge and whether it is either a lifted or a strong base edge. If so, the optimal solution is either (i) all edges except the two largest ones or (ii) all edges, whichever gives smaller objective value. If the above condition does not hold, the optimal solution can be chosen to contain all negative edges.

We use a variation of the path optimization algorithm with an edge fixed to 0 or 1 for computing min-marginals.

**Cutting plane.** Since there are exponentially many path

subproblems, we add during the optimization only those that improve the relaxation. Details are in Appendix 8.4.

### 4.4. Cut Subproblems

The purpose of a cut subproblem is to reflect that a lifted edge  $uv$  must be labelled 0 if there exists a cut of base edges that separate  $u$  and  $v$  ( $uv$ -cut) all labelled 0.

**The feasible set.** A cut subproblem consists of a lifted edge  $uv$  and a  $uv$ -cut  $C = \{ij \in E \mid i \in A, j \in B\}$  where  $A, B \subset V$  with  $A \cap B = \emptyset$ . The space of feasible solutions  $\mathcal{X}^C$  is defined as

$$\begin{aligned} y'_{uv} \in \{0, 1\}, y \in \{0, 1\}^C : \quad & y'_{uv} \leq \sum_{ij \in C} y_{ij}, \\ \forall i \in A : \sum_{ij \in C} y_{ij} \leq 1, \quad \forall j \in B : \sum_{ij \in C} y_{ij} \leq 1, \\ uv \in C \Rightarrow & y'_{uv} \geq y_{uv}. \end{aligned} \quad (10)$$

The constraints stipulate that (i) the lifted edge  $uv$  is 0 if all the edges in the cut are 0, (ii) there exists at most one active outgoing resp. incoming edge for every vertex in  $A$  resp.  $B$  and (iii) if there is also base edge  $uv \in C$  then whenever it is active, the lifted edge  $uv$  must be active.

---

#### Algorithm 3 Cut-Subproblem-Optimization

---

**Input** Edge costs  $\theta^C$

**Output** optimal value  $\text{opt}$  of subproblem.

- 1: Define  $\psi \in \mathbb{R}^{A \times B}$ :
  - 2:  $\psi_{ij} = \begin{cases} \theta_{uv}^C + \theta_{uv}'^C, & \text{if } ij = uv \wedge uv \in C \wedge \theta_{uv}'^C > 0 \\ \infty, & \text{if } ij \notin C \\ \theta_{ij}^C, & \text{otherwise} \end{cases}$
  - 3:  $z^* \in \underset{z \in \{0, 1\}^{A \times B}}{\text{argmin}} \sum_{i \in A} \sum_{j \in B} \psi_{ij} z_{ij}$ , s.t.  $z \mathbf{1} \leq \mathbf{1}, z^\top \mathbf{1} \leq \mathbf{1}$
  - 4:  $\text{opt} = \sum_{ij \in C} \psi_{ij} z_{ij}^*$
  - 5: **if**  $\theta_{uv}'^C \geq 0$  **then** return  $\text{opt}$
  - 6: **if**  $\exists kl \in C : z_{kl} = 1$  **then**
  - 7:     return  $\text{opt} + \theta_{uv}'^C$
  - 8: **else**
  - 9:      $\alpha = \min_{ij \in C} \theta_{ij}^C$
  - 10:    **if**  $|\theta_{uv}'^C| > \alpha$  **then** return  $\theta_{uv}'^C + \alpha$
  - 11:    **else** return  $\text{opt}$
  - 12: **end if**
- 

**Optimization of a cut subproblem** with respect to feasible set  $\mathcal{X}^C$  is given by Alg. 3. Its key is to solve a linear assignment problem (LAP) [1] between vertex sets  $A$  and  $B$ . The assignment cost  $\psi_{ij}$  for  $(i, j) \in A \times B$  is the cut edge cost  $\theta_{ij}^C$  if edge  $ij$  belongs to  $C$  and  $\infty$  otherwise. In the special case of  $uv$ -cut  $C$  containing base edge  $uv$  and the lifted edge cost  $\theta_{uv}'^C$  being positive, the assignment cost  $\psi_{uv}$  is increased by  $\theta_{uv}'^C$ .

A candidate optimal labeling of cut edges is given by values of LAP variables  $z_{ij}$ . If  $\theta_{uv}'^C \geq 0$ , the optimal value

found by the LAP is the optimal value of the cut subproblem. If it is negative, we distinguish two cases: (i) If a cut edge  $kl$  labeled by one exists, the lifted edge cost  $\theta_{uv}^C$  is added to the optimal value of LAP. (ii) Otherwise, we inspect whether it is better to activate the smallest-cost cut edge and the lifted edge  $uv$  or keep all edges inactive.

We use a variation of Alg. 3 with an edge variable restricted to be either 0 or 1 for computing min-marginals.

**Cutting plane.** There are exponentially many cut subproblems. Therefore, we add only those that improve the lower bound. See Appendix 8.5 for details.

#### 4.5. Message Passing

The overall algorithm for optimizing the Lagrange decomposition is Alg. 19 in the Appendix. First, inflow and outflow subproblems are initialized for every node. Then, for a number of iterations or until convergence, costs for each subproblems are adjusted iteratively by computing min-marginals and adjusting the reparametrization proportionally to the min-marginal’s value. Additionally, every  $k$ -th iteration additional path and cut subproblems are separated and added to the Lagrange decomposition.

**Solver complexity.** We need  $\mathcal{O}(|E^{inp}|)$  space where  $E^{inp}$  are all edges before graph sparsification. The most time consuming is computing lifted edges min-marginals for each in/outflow subproblem. Alg. 6 computes them for one outflow subproblem and it is linear in the number of detections per frame. This significantly improves the complexity of to the optimal LDP solver Lift, making LDP applicable to large problem instances. See Appendix 8.14 for details.

#### 4.6. Primal Rounding

For computing primal solutions we solve a minimum cost flow (MCF) problem on the base edges and improve this initial solution with a local search heuristic.

Without lifted edges, the disjoint paths problem is an instance of MCF, which can be efficiently optimized via combinatorial solvers like the successive shortest path solver that we employ [1]. We enforce node disjoint paths via splitting each node  $u \in V$  into two nodes  $u^{in}, u^{out} \in V^{mcf}$  in the MCF graph  $G^{mcf} = (V^{mcf}, E^{mcf})$ , adding an additional edge  $u^{in}u^{out}$  to  $E^{mcf}$  and setting capacity  $[0, 1]$  on all edges  $E^{mcf}$ . Each node except  $s$  and  $t$  has demand 0. Alg. 4 calculates MCF edge costs from in/outflow subproblems using Alg. 1. We obtain the cost of each flow edge  $w^{out}v^{in}$  from the inflow subproblem of  $v$  and the outflow subproblem of  $u$  using their minima where edge  $uv$  is active. This combines well the cost from base and lifted edges.

We describe the local search heuristic for improving the MCF solution in Alg. 25 in the Appendix. It works with sets of disjoint paths. First, paths are split if this leads to a decrease in the objective. Second, merges are explored. If a merge of two paths is not possible, we iteratively check

whether cutting off one node from the first path’s end or the second paths’s beginning makes the connection possible. If yes and the connection is decreasing the objective, the nodes are cut off and the paths are connected.

---

#### Algorithm 4 Init-MCF

---

- 1:  $\forall u \in V \setminus \{s, t\}$ :  
 $(\alpha, lc, \alpha^{in}) = \text{Opt-In-Cost}(u, \theta_u^{in})$   
 $(\alpha, lc, \alpha^{out}) = \text{Opt-Out-Cost}(u, \theta_u^{out})$
  - 2:  $\forall u \in V \setminus \{s, t\} : \theta_{su^{in}}^{mcf} = \alpha_{su}^{in}, \theta_{u^{out}t}^{mcf} = \alpha_{ut}^{out}$
  - 3:  $\forall u \in \{uv \in E | u \neq s, v \neq t\} : \theta_{u^{out}v^{in}}^{mcf} = \alpha_{uv}^{out} + \alpha_{uv}^{in}$
- 

## 5. Experiments

We integrate our LDP solver into an MOT system (Appendix, Fig. 1) and show on challenging datasets that higher order MOT is scalable to big problem instances. In the next sections, we describe our experimental setup and present results. We clarify the edge cost calculation and construction of the base and the lifted graph and their sparsification.

### 5.1. Pairwise Costs

We use multi layer perceptrons (MLP) to predict the likelihood that two detections belong to the same trajectory. We divide the maximal frame distance into 20 intervals of equal length and train one separate MLP for each set of frame distances. We transform the MLP output to the cost of the edge between the detections and use it in our objective (3). Negative cost indicates that two detections belong to the same trajectory. Positive cost reflects the opposite.

**MLP architecture.** Each MLP consists of a fully connected layer with the same number of neurons as the input size, followed by a LeakyReLU activation [43] and a fully connected single neuron output layer. We add sigmoid activation in the training. We describe our spatial and visual features used as the input in the paragraphs below.

**Spatial feature** uses bounding box information of two detections  $v$  and  $w$ . We align the boxes such that their centers overlap. The similarity feature  $\sigma_{vw, \text{Spa}} \in [0, 1]$  is the intersection-over-union between two aligned boxes.

**Appearance feature.** We create an appearance feature  $F_v$  for each detection  $v$  by training the method [67] on the training set of the respective benchmark and additional data from [66, 59, 50]. The similarity feature  $\sigma_{vw, \text{App}}$  between detection  $v$  and  $w$  given by  $\sigma_{vw, \text{App}} := \max\{0, \langle F_v, F_w \rangle\}$  is used. A higher value indicates a higher similarity.

**Global context normalization.** The two features  $\sigma_{vw, \text{Spa}}, \sigma_{vw, \text{App}}$  depend entirely on the nodes  $v$  and  $w$ . To include global context, we append several normalized versions of the two features to the edge feature vector, inspired by [28]. Both features  $\sigma_{ij, *}$  of edge  $ij$  undergo a five-way normalization. In each case, the maximum feature value from a rel-

evant set of edges is selected as the normalization value. The normalization is done by dividing the two features  $\sigma_{ij,*}$  by each of their five normalization values. This yields 10 values. Another set of 10 values for edge  $ij$  is obtained by dividing  $\sigma_{ij,*}^2$  by each of the five normalization values. Together with the two unnormalized features  $\sigma_{ij,*}$ , edge feature vectors have length 22. See Appendix 8.9 for details.

**Training.** We iteratively train our MLP on batches  $B$  containing sampled edges. To compensate the imbalance between true positive and true negative edges, we use an  $\alpha$ -balanced focal loss [40] with  $\gamma = 1$ . We define the  $\alpha$ -weight  $\alpha^{(g,\Delta f)}$  to weight the correct classification of edge  $vw$  with ground truth flow value  $g_{vw} \in \{0, 1\}$ , time distance  $\Delta f$  between  $v$  in frame  $f_v$  and  $w$  in frame  $f_w$ , and value  $g \in \{0, 1\}$  via  $\alpha^{(g,\Delta f)} := 1/|\{vw \in E : |f_v - f_w| = \Delta f, g_{vw} = g\}|$ . We optimize the classifier using Adam with  $l_r = 0.1$ ,  $\beta_1 = 0.9$ ,  $\beta_2 = 0.999$  and  $\epsilon = 10^{-8}$ . To reduce complexity while maintaining variety during training, we introduce an extended sampling. Given a frame  $f$ , we create batches  $B(f)$  by sampling detections from a fixed sequence of frame shifts starting at frame  $f$  ensuring that all temporal distances  $\Delta f$  are present in  $B(f)$  (details in Appendix 8.11). We then subsample the  $k$ -nearest detections to a random generated image position with  $k = 160$ , which sensitizes training to crowded scenes. We train the MLP for 3 epochs with batches  $B(f)$  for all frames  $f$  of the dataset.

## 5.2. Graph Construction

We create the base and the lifted graph edges between detections with time distance up to 2 seconds. We also add an edge from source  $s$ , and to sink  $t$  to each detection. In order to reduce computational complexity, we apply sparsification on both base and lifted graph as described later.

**Costs.** We obtain base and lifted costs  $c$  and  $c'$  from the same MLP classifier (Sec. 5.1). Due to decreasing classification accuracy with increasing frame distance  $\Delta f$ , we multiply the costs by a decay weight  $\omega_{\Delta f} := (10 \cdot \Delta f + 0.1)^{-1}$ , so that edges representing long temporal distances have lower weight. Edges from  $s$  and to  $t$  have costs zero.

Finally, we use simple heuristics to find pairs that are obviously matching or non-matching. We set the corresponding costs to be high in absolute value, negative for matching and positive for non-matching, thereby inducing soft constraints. An obvious match is given by a nearly maximal feature similarity. Detection pairs are obviously non-matching, if the displacement between their bounding boxes is too high. See Appendix 8.12 for details.

**Sparsification.** The base edges are an intersection of two edge sets. The first set contains for every  $v \in V'$  edges to its 3 nearest (lowest-cost) neighbors from every subsequent time frame. The second set selects for every vertex the best edges to its preceding frames analogically. Moreover, edges longer than 6 frames must have costs lower than 3.0. To

avoid double counting of edge costs, we subsequently set costs of all base edges between non-consecutive frames to zero, so that only lifted edges maintain the costs. If a lifted edge has cost around zero, it is not discriminative and we remove it, unless it overlaps with a (zero-valued) base edge.

## 5.3. Inference

For fair comparison to state of the art, we filter and refine detections using tracktor [7] as in [28]. Different to [28], we apply tracktor to recover missing detections before running the solver.

While we solve MOT15/16/17 on global graphs, we solve MOT20 in time intervals in order to decrease memory consumption and runtime. First, we solve the problem on non-overlapping adjacent intervals and fix the trajectories in the interval centers. Second, we solve the problem on a new set of intervals where each of them covers unassigned detections in two initial neighboring intervals and enables connections to the fixed trajectory fragments. We use the maximal edge length of 50 frames in MOT20. Therefore, 150 is the minimal interval length such that all edges from a detection are used when assigning the detection to a trajectory. This way, the solver has sufficient context for making each decision. Intervals longer than 200 frames increase the complexity significantly for MOT20, therefore we use interval length 150 in our experiments.

**Post-processing.** We use simple heuristics to check if base edges over long time gaps correspond to plausible motions, and split trajectories if necessary. Finally, we use linear interpolation to recover missing detections within a trajectory. Appendix 8.13 contains further details on inference.

## 5.4. Tracking Evaluation

We evaluate our method on four standard MOT benchmarks. The MOT15/16/17 benchmarks [37, 45] contain semi-crowded videos sequences filmed from a static or a moving camera. MOT20 [16] comprises crowded scenes with considerably higher number of frames and detections per frame, see Tab. 1. The challenge does not come only with the data size. Detectors make more errors in crowded scenes due to frequent occlusions and appearance features are less discriminative as the distance of people to the camera is high. Using higher order information helps in this context. However, the number of edges in our graphs grows quadratically with the number of detections per frame. Therefore, it is crucial to make the tracker scalable to these massive data. We use the following ingredients to solve the problems: (i) fast but accurate method for obtaining edge costs, (ii) approximate LDP solver delivering high-quality results fast, (iii) preprocessing heuristics, (iv) interval solution keeping sufficient context for each decision.

We use training data of the corresponding dataset for training and the public detections for training and test.

Table 1. Comparison of ApLift with the best performing solvers w.r.t. MOTA metric on the MOT challenge.  $\uparrow$  higher is better,  $\downarrow$  lower is better. The two rightmost columns: average number of frames per sequence and the average number of detections per frame for dataset.

	Method	MOTA $\uparrow$	IDF1 $\uparrow$	MT $\uparrow$	ML $\downarrow$	FP $\downarrow$	FN $\downarrow$	IDS $\downarrow$	Frag $\downarrow$	Frames	Density
MOT20	ApLift (ours)	<b>58.9</b>	56.5	<b>513</b>	<b>264</b>	17739	<b>192736</b>	2241	2112		
	MPNTrack [10]	57.6	<b>59.1</b>	474	279	16953	201384	<b>1210</b>	<b>1420</b>	1119.8	170.9
	Tracktor++v2 [7]	52.6	52.7	365	331	<b>6930</b>	236680	1648	4374		
MOT17	CTTrackPub [68]	<b>61.5</b>	59.6	621	752	<b>14076</b>	200672	2583	4965		
	ApLift (ours)	60.5	<b>65.6</b>	<b>798</b>	<b>728</b>	30609	<b>190670</b>	1709	2672	845.6	31.8
	Lif_T [28]	60.5	<b>65.6</b>	637	791	14966	206619	1189	3476		
	MPNTrack [10]	58.8	61.7	679	788	17416	213594	<b>1185</b>	<b>2265</b>		
MOT16	ApLift (ours)	<b>61.7</b>	<b>66.1</b>	<b>260</b>	<b>237</b>	9168	<b>60180</b>	495	802		
	Lif_T [28]	61.3	64.7	205	258	4844	65401	389	1034	845.6	30.8
	MPNTrack [10]	58.6	61.7	207	258	4949	70252	<b>354</b>	<b>684</b>		
	GSM [41]	57.0	55.0	167	262	<b>4332</b>	73573	475	859		
MOT15	Lif_T [28]	<b>52.5</b>	<b>60.0</b>	244	186	6837	21610	730	1047		
	MPNTrack [10]	51.5	58.6	225	187	7260	21780	<b>375</b>	<b>872</b>	525.7	10.8
	ApLift (ours)	51.1	59.0	<b>284</b>	<b>163</b>	10070	<b>19288</b>	677	1022		
	Tracktor15 [7]	44.1	46.7	130	189	<b>6477</b>	26577	1318	1790		

Table 2. Influence of lifted graph sparsification, message passing and using zero base costs on MOT17 train without postprocessing.

$E'$	MP steps	Base cost	IDF1 $\uparrow$	MOTA $\uparrow$	FP $\downarrow$	FN $\downarrow$	IDS $\downarrow$
Dense	82	Zero	<b>71.0</b>	<b>66.3</b>	2826	<b>109263</b>	1369
Dense	0	Zero	70.3	<b>66.3</b>	2832	109265	1354
Dense	82	Orig.	69.8	<b>66.3</b>	<b>2824</b>	109266	1355
Sparse	82	Orig.	69.1	<b>66.3</b>	2825	<b>109263</b>	<b>1316</b>

Table 3. Runtime and IDF1 comparison of LDP solvers: ApLift (ours) with 6, 11, 31 and 51 iterations and LifT[28] (two step procedure) on first  $n$  frames of sequence *MOT20-01* from MOT20.

$n$	Measure	LifT	Our6	Our11	Our31	Our51
50	IDF1 $\uparrow$	80.6	<b>83.3</b>	<b>83.3</b>	81.5	81.5
	time [s]	272	2	4	16	35
100	IDF1 $\uparrow$	80.4	<b>82.5</b>	<b>82.5</b>	81.6	81.6
	time [s]	484	14	24	97	218
150	IDF1 $\uparrow$	78.1	<b>81.0</b>	<b>81.0</b>	79.8	79.8
	time [s]	1058	25	46	192	431
200	IDF1 $\uparrow$	73.2	<b>75.4</b>	<b>75.4</b>	74.6	74.6
	time [s]	2807	36	66	277	616

We compare our method using standard MOT metrics. MOTA [8] and IDF1 [49] are considered the most representative as they incorporate other metrics (in particular recall and precision). IDF1 is more penalized by inconsistent trajectories. We also report mostly tracked (MT) and mostly lost trajectories (ML), false negatives (FN) and false positives (FP), ID switches (IDS) and fragmentations (Frag) as provided by the evaluation protocols [8] of the benchmarks.

Tab. 1 shows the comparison to the best (w.r.t. MOTA) peer-reviewed methods on test sets. Our approximate solver achieves almost the same results on MOT15/16/17 as the optimal LDP solver [28], while using simpler features. Overall, our method performs on par with state of the art on all evaluated benchmarks, especially in MOTA and IDF1. Our complete results and videos are publicly available<sup>3</sup>. The proposed method achieves overall low FN values but

<sup>3</sup><https://motchallenge.net/method/MOT=4031&chl=13>

slightly high FP values. FP/FN are mostly affected by pre-processing the input detections and interpolation in the post-processing. The impact of post-processing (trajectory splits and interpolations) on MOT20, which causes FP but reduces FN and IDS, is analyzed in the Appendix (Tab. 4).

Tab. 2 shows the influence of various settings on the performance of MOT17 train. While we usually set the base edge costs to zero (Sec. 5.2), we need to keep them when using the sparsified lifted graph. Both, message passing and dense lifted edges improve IDF1 and IDS. However, MOTA, FN and FP remain almost unchanged.

Finally, we compare the runtime of our solver against the two step version of LifT for a sample sequence in Tab. 3. With increasing problem complexity, our solver outperforms LifT w.r.t. runtime while achieving similar IDF1. Counter-intuitively, as we progress towards increasingly better optimization objective values, the tracking metrics can slightly decrease due to imperfect edge costs. We compare our solver against optimal (one step) LifT on MOT17 train in Appendix 8.14.

## 6. Conclusion

We demonstrated that the NP-hard LDP model is applicable for processing massive sequences of MOT20. The combination of an approximate LDP solver, efficiently computable costs and subdivision of data keeping sufficient context for each decision make this possible.

## 7. Acknowledgements

This work was supported by the Federal Ministry of Education and Research (BMBF), Germany, under the project LeibnizKILabor (grant no. 01DD20003), the Center for Digital Innovations (ZDIN) and the Deutsche Forschungsgemeinschaft (DFG) under Germany’s Excellence Strategy within the Cluster of Excellence PhoenixD (EXC 2122).



## References

- [1] Ravindra K Ahuja, Thomas L Magnanti, and James B Orlin. *Network flows*. Cambridge, Mass.: Alfred P. Sloan School of Management, Massachusetts, 1988. 5, 6
- [2] Alexandre Alahi, Yannick Boursier, Laurent Jacques, and Pierre Vanderghenst. Sport players detection and tracking with a mixed network of planar and omnidirectional cameras. In *2009 Third ACM/IEEE International Conference on Distributed Smart Cameras (ICDSC)*, pages 1–8. IEEE, 2009. 1
- [3] Alexandre Alahi, Judson Wilson, Li Fei-Fei, and Silvio Savarese. Unsupervised camera localization in crowded spaces. In *2017 IEEE International Conference on Robotics and Automation (ICRA)*, pages 2666–2673. IEEE, 2017. 1
- [4] Chetan Arora and Amir Globerson. Higher order matching for consistent multiple target tracking. In *Proceedings of the IEEE International Conference on Computer Vision*, pages 177–184, 12 2013. 2
- [5] Maryam Babaei, Ali Athar, and Gerhard Rigoll. Multiple people tracking using hierarchical deep tracklet re-identification. *arXiv preprint arXiv:1811.04091*, 2018. 2
- [6] Jerome Berclaz, Francois Fleuret, Engin Turetken, and Pascal Fua. Multiple object tracking using k-shortest paths optimization. *IEEE Transactions on Pattern Analysis and Machine Intelligence*, 33(9):1806–1819, 2011. 2
- [7] Philipp Bergmann, Tim Meinhardt, and Laura Leal-Taixé. Tracking without bells and whistles. In *IEEE International Conference on Computer Vision*, pages 941–951, 2019. 2, 7, 8
- [8] Keni Bernardin and Rainer Stiefelhagen. Evaluating multiple object tracking performance: The clear mot metrics. *EURASIP Journal on Image and Video Processing*, 2008, 01 2008. 8
- [9] Erik Bochinski, Volker Eiselein, and Thomas Sikora. High-speed tracking-by-detection without using image information. In *2017 14th IEEE International Conference on Advanced Video and Signal Based Surveillance (AVSS)*, pages 1–6. IEEE, 2017. 2
- [10] Guillem Brasó and Laura Leal-Taixé. Learning a neural solver for multiple object tracking. In *Proceedings of the IEEE/CVF Conference on Computer Vision and Pattern Recognition*, pages 6247–6257, 2020. 2, 8
- [11] William Brendel, Mohamed Amer, and Sinisa Todorovic. Multiobject tracking as maximum weight independent set. In *IEEE Conference on Computer Vision and Pattern Recognition*, pages 1273–1280. IEEE, 2011. 2
- [12] Visesh Chari, Simon Lacoste-Julien, Ivan Laptev, and Josef Sivic. On pairwise costs for network flow multi-object tracking. In *IEEE Conference on Computer Vision and Pattern Recognition*, pages 5537–5545, 2015. 2
- [13] Chee-Yee Chong, Shozo Mori, and Donald B Reid. Forty years of multiple hypothesis tracking—a review of key developments. In *2018 21st International Conference on Information Fusion (FUSION)*, pages 452–459. IEEE, 2018. 2
- [14] Sunil Chopra and Mendu R Rao. The partition problem. *Mathematical Programming*, 59(1):87–115, 1993. 2, 5
- [15] Afshin Dehghan, Shayan Modiri Assari, and Mubarak Shah. GMMCP tracker: Globally optimal generalized maximum multi clique problem for multiple object tracking. In *IEEE Conference on Computer Vision and Pattern Recognition*, pages 4091–4099, 2015. 2
- [16] Patrick Dendorfer, Hamid Reza Tofighi, Anton Milan, Javen Shi, Daniel Cremers, Ian Reid, Stephan Roth, Konrad Schindler, and Laura Leal-Taixé. Mot20: A benchmark for multi object tracking in crowded scenes. *arXiv:2003.09003[cs]*, Mar. 2020. arXiv: 2003.09003. 2, 7, 24, 28, 30
- [17] Kaiwen Duan, Song Bai, Lingxi Xie, Honggang Qi, Qingming Huang, and Qi Tian. Centernet: Keypoint triplets for object detection. In *Proceedings of the IEEE/CVF International Conference on Computer Vision*, pages 6569–6578, 2019. 1
- [18] Michele Fenzi, Jörn Ostermann, Nico Mentzer, Guillermo Payá-Vayá, Holger Blume, Tu Ngoc Nguyen, and Thomas Risse. Asev—automatic situation assessment for event-driven video analysis. In *2014 11th IEEE International Conference on Advanced Video and Signal Based Surveillance (AVSS)*, pages 37–43. IEEE, 2014. 1
- [19] Davi Frossard and Raquel Urtasun. End-to-end learning of multi-sensor 3d tracking by detection. In *2018 IEEE international conference on robotics and automation (ICRA)*, pages 635–642. IEEE, 2018. 1
- [20] Amir Globerson and Tommi Jaakkola. Fixing max-product: Convergent message passing algorithms for map lp-relaxations. *Advances in neural information processing systems*, 20:553–560, 2007. 2
- [21] Monique Guignard and Siwhan Kim. Lagrangean decomposition for integer programming: theory and applications. *RAIRO-Operations Research-Recherche Opérationnelle*, 21(4):307–323, 1987. 3
- [22] LLC Gurobi Optimization. Gurobi optimizer reference manual, 2019. 2
- [23] Roberto Henschel, Laura Leal-Taixé, Daniel Cremers, and Bodo Rosenhahn. Fusion of head and full-body detectors for multi-object tracking. In *IEEE Conference on Computer Vision and Pattern Recognition Workshops*, June 2018. 2
- [24] Roberto Henschel, Timo von Marcard, and Bodo Rosenhahn. Simultaneous identification and tracking of multiple people using video and imus. In *Proceedings of the IEEE Conference on Computer Vision and Pattern Recognition Workshops*, pages 0–0, 2019. 2
- [25] Roberto Henschel, Yunzhe Zou, and Bodo Rosenhahn. Multiple people tracking using body and joint detections. In *IEEE Conference on Computer Vision and Pattern Recognition Workshops*, pages 0–0, 2019. 2
- [26] Kalun Ho, Amirhossein Kardoost, Franz-Josef Pfreundt, Janis Keuper, and Margret Keuper. A two-stage minimum cost multicut approach to self-supervised multiple person tracking. In *Proceedings of the Asian Conference on Computer Vision (ACCV)*, November 2020. 2
- [27] Martin Hofmann, Daniel Wolf, and Gerhard Rigoll. Hypergraphs for joint multi-view reconstruction and multi-object tracking. In *IEEE Conference on Computer Vision and Pattern Recognition*, pages 3650–3657, 2013. 2

- [28] Andrea Hornakova, Roberto Henschel, Bodo Rosenhahn, and Paul Swoboda. Lifted disjoint paths with application in multiple object tracking. In *The 37th International Conference on Machine Learning (ICML)*, July 2020. 1, 2, 3, 6, 7, 8, 27, 28, 29
- [29] Andrea Horňáková, Jan-Hendrik Lange, and Bjoern Andres. Analysis and optimization of graph decompositions by lifted multicuts. In *International Conference on Machine Learning*, 2017. 2
- [30] Weiming Hu, Xinchu Shi, Zongwei Zhou, Junliang Xing, Haibin Ling, and Stephen Maybank. Dual L1-normalized context aware tensor power iteration and its applications to multi-object tracking and multi-graph matching. *International Journal of Computer Vision*, Oct 2019. 2
- [31] Chang Huang, Bo Wu, and Ramakant Nevatia. Robust object tracking by hierarchical association of detection responses. In *European Conference on Computer Vision*, pages 788–801. Springer, 2008. 2
- [32] Hao Jiang, Sidney Fels, and James J Little. A linear programming approach for multiple object tracking. In *2007 IEEE Conference on Computer Vision and Pattern Recognition*, pages 1–8. IEEE, 2007. 2
- [33] Margret Keuper, Siyu Tang, Bjoern Andres, Thomas Brox, and Bernt Schiele. Motion segmentation & multiple object tracking by correlation co-clustering. *IEEE Transactions on Pattern Analysis and Machine Intelligence*, 42(1):140–153, 2018. 2
- [34] Chanho Kim, Fuxin Li, Arridhana Ciptadi, and James M Rehg. Multiple hypothesis tracking revisited. In *Proceedings of the IEEE international conference on computer vision*, pages 4696–4704, 2015. 2
- [35] Péter Kovács. Minimum-cost flow algorithms: an experimental evaluation. *Optimization Methods and Software*, 30(1):94–127, 2015. 1, 2
- [36] Ratnesh Kumar, Guillaume Charpiat, and Monique Thonnat. Multiple object tracking by efficient graph partitioning. In *Asian Conference on Computer Vision*, pages 445–460. Springer, 2014. 2
- [37] Laura Leal-Taixé, Anton Milan, Ian Reid, Stephan Roth, and Konrad Schindler. MOTChallenge 2015: Towards a benchmark for multi-target tracking. *arXiv:1504.01942 [cs]*, Apr. 2015. arXiv: 1504.01942. 2, 7
- [38] Laura Leal-Taixé, Gerard Pons-Moll, and Bodo Rosenhahn. Branch-and-price global optimization for multi-view multi-target tracking. In *IEEE Conference on Computer Vision and Pattern Recognition*, pages 1987–1994. IEEE, 2012. 2
- [39] Ming Liang, Bin Yang, Wenyuan Zeng, Yun Chen, Rui Hu, Sergio Casas, and Raquel Urtasun. Pnpnet: End-to-end perception and prediction with tracking in the loop. In *Proceedings of the IEEE/CVF Conference on Computer Vision and Pattern Recognition*, pages 11553–11562, 2020. 1
- [40] Tsung-Yi Lin, Priyal Goyal, Ross Girshick, Kaiming He, and Piotr Dollar. Focal loss for dense object detection. *IEEE Transactions on Pattern Analysis and Machine Intelligence*, PP:1–1, 07 2018. 7
- [41] Qiankun Liu, Qi Chu, Bin Liu, and Nenghai Yu. Gsm: Graph similarity model for multi-object tracking. In Christian Bessiere, editor, *Proceedings of the Twenty-Ninth International Joint Conference on Artificial Intelligence, IJCAI-20*, pages 530–536. International Joint Conferences on Artificial Intelligence Organization, 7 2020. Main track. 8
- [42] Wei-Lwun Lu, Jo-Anne Ting, James J Little, and Kevin P Murphy. Learning to track and identify players from broadcast sports videos. *IEEE transactions on pattern analysis and machine intelligence*, 35(7):1704–1716, 2013. 1
- [43] Andrew L. Maas, Awny Y. Hannun, and Andrew Y. Ng. Rectifier nonlinearities improve neural network acoustic models. In *Proceedings of the International Conference on Machine Learning*, Atlanta, Georgia, 2013. 6, 23, 24
- [44] Florian Meyer, Thomas Kropfpreiter, Jason L Williams, Roslyn Lau, Franz Hlawatsch, Paolo Braca, and Moe Z Win. Message passing algorithms for scalable multitarget tracking. *Proceedings of the IEEE*, 106(2):221–259, 2018. 2
- [45] Anton Milan, Laura Leal-Taixé, Ian Reid, Stephan Roth, and Konrad Schindler. MOT16: A benchmark for multi-object tracking. *arXiv:1603.00831 [cs]*, Mar. 2016. arXiv: 1603.00831. 2, 7, 28, 30
- [46] Joseph Redmon, Santosh Divvala, Ross Girshick, and Ali Farhadi. You only look once: Unified, real-time object detection. In *Proceedings of the IEEE conference on computer vision and pattern recognition*, pages 779–788, 2016. 1
- [47] Shaoqing Ren, Kaiming He, Ross Girshick, and Jian Sun. Faster r-cnn: Towards real-time object detection with region proposal networks. *arXiv preprint arXiv:1506.01497*, 2015. 1
- [48] Seyed Hamid Rezaatofighi, Anton Milan, Zhen Zhang, Qinfeng Shi, Anthony Dick, and Ian Reid. Joint probabilistic data association revisited. In *Proceedings of the IEEE international conference on computer vision*, pages 3047–3055, 2015. 2
- [49] Ergys Ristani, Francesco Solera, Roger Zou, Rita Cucchiara, and Carlo Tomasi. Performance measures and a data set for multi-target, multi-camera tracking. In Gang Hua and Hervé Jégou, editors, *Computer Vision – ECCV 2016 Workshops*, pages 17–35, Cham, 2016. Springer International Publishing. 8
- [50] Ergys Ristani, Francesco Solera, Roger S. Zou, Rita Cucchiara, and Carlo Tomasi. Performance measures and a data set for multi-target, multi-camera tracking. In *European Conference on Computer Vision Workshop on Benchmarking Multi-Target Tracking*, 2016. 6
- [51] Ergys Ristani and Carlo Tomasi. Tracking multiple people online and in real time. In *Asian Conference on Computer Vision*, pages 444–459. Springer, 2014. 2
- [52] Amir Sadeghian, Alexandre Alahi, and Silvio Savarese. Tracking the untrackable: Learning to track multiple cues with long-term dependencies. In *IEEE International Conference on Computer Vision*, pages 300–311, 2017. 2
- [53] Julian Smith, Florian Particke, Markus Hiller, and Jörn Thielecke. Systematic analysis of the pmbm, phd, jpda and gnn multi-target tracking filters. In *2019 22th International Conference on Information Fusion (FUSION)*, pages 1–8, 2019. 2

- [54] Paul Swoboda, Jan Kuske, and Bogdan Savchynskyy. A dual ascent framework for lagrangean decomposition of combinatorial problems. In *Proceedings of the IEEE Conference on Computer Vision and Pattern Recognition (CVPR)*, July 2017. 2, 3, 4
- [55] Siyu Tang, Bjoern Andres, Mykhaylo Andriluka, and Bernt Schiele. Subgraph decomposition for multi-target tracking. In *IEEE Conference on Computer Vision and Pattern Recognition*, pages 5033–5041, 2015. 2
- [56] Siyu Tang, Bjoern Andres, Mykhaylo Andriluka, and Bernt Schiele. Multi-person tracking by multicut and deep matching. In *European Conference on Computer Vision*, pages 100–111. Springer, 2016. 1, 2
- [57] Siyu Tang, Mykhaylo Andriluka, Bjoern Andres, and Bernt Schiele. Multiple people tracking by lifted multicut and person re-identification. In *IEEE Conference on Computer Vision and Pattern Recognition*, 2017. 1, 2
- [58] Timo von Marcard, Roberto Henschel, Michael J Black, Bodo Rosenhahn, and Gerard Pons-Moll. Recovering accurate 3d human pose in the wild using imus and a moving camera. In *Proceedings of the European Conference on Computer Vision (ECCV)*, pages 601–617, 2018. 2
- [59] Longhui Wei, Shiliang Zhang, Wen Gao, and Qi Tian. Person transfer gan to bridge domain gap for person re-identification. In *IEEE Conference on Computer Vision and Pattern Recognition*, pages 79–88, 2018. 6
- [60] Nicolai Wojke and Alex Bewley. Deep cosine metric learning for person re-identification. In *2018 IEEE Winter Conference on Applications of Computer Vision (WACV)*, pages 748–756. IEEE, 2018. 2
- [61] Nicolai Wojke, Alex Bewley, and Dietrich Paulus. Simple online and realtime tracking with a deep association metric. In *2017 IEEE International Conference on Image Processing (ICIP)*, pages 3645–3649. IEEE, 2017. 2
- [62] Jiarui Xu, Yue Cao, Zheng Zhang, and Han Hu. Spatial-temporal relation networks for multi-object tracking. In *IEEE International Conference on Computer Vision*, pages 3988–3998, 2019. 2
- [63] Fan Yang, Wongun Choi, and Yuanqing Lin. Exploit all the layers: Fast and accurate cnn object detector with scale dependent pooling and cascaded rejection classifiers. In *Proceedings of the IEEE conference on computer vision and pattern recognition*, pages 2129–2137, 2016. 1
- [64] Amir Roshan Zamir, Afshin Dehghan, and Mubarak Shah. GMCP-tracker: Global multi-object tracking using generalized minimum clique graphs. In *European Conference on Computer Vision*, pages 343–356. Springer, 2012. 2
- [65] Li Zhang, Yuan Li, and Ramakant Nevatia. Global data association for multi-object tracking using network flows. In *IEEE Conference on Computer Vision and Pattern Recognition*, pages 1–8. IEEE, 2008. 1, 2
- [66] Liang Zheng, Liyue Shen, Lu Tian, Shengjin Wang, Jingdong Wang, and Qi Tian. Scalable person re-identification: A benchmark. In *IEEE International Conference on Computer Vision*, pages 1116–1124, 2015. 6
- [67] Zhedong Zheng, Xiaodong Yang, Zhiding Yu, Liang Zheng, Yi Yang, and Jan Kautz. Joint discriminative and generative learning for person re-identification. In *IEEE Conference on Computer Vision and Pattern Recognition*, 2019. 6
- [68] Xingyi Zhou, Vladlen Koltun, and Philipp Krähenbühl. Tracking objects as points. In *European Conference on Computer Vision*, pages 474–490. Springer, 2020. 2, 8
- [69] Ji Zhu, Hua Yang, Nian Liu, Minyoung Kim, Wenjun Zhang, and Ming-Hsuan Yang. Online multi-object tracking with dual matching attention networks. In *European Conference on Computer Vision*, pages 366–382, 2018. 2

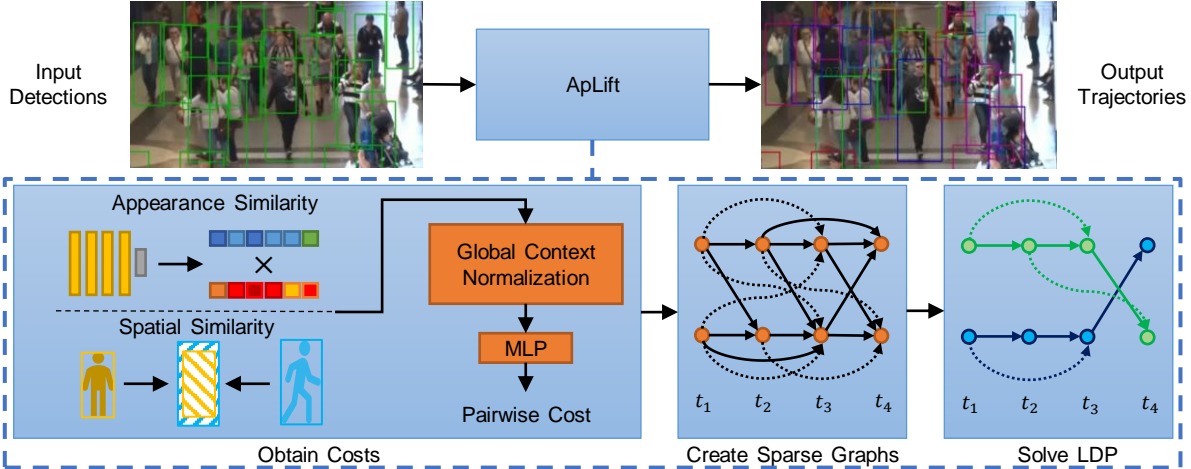


Figure 1. Overview of the ApLift framework. Input detections are used to obtain pairwise costs by an MLP with spatial and appearance features. Based on the costs, two sparse graphs are constructed and passed to our proposed approximate LDP solver. Dashed arrows represent lifted edges and solid arrows base edges. In figure *Solve LDP* equally colored nodes and edges belong to the same trajectory.

## 8. Appendix

This Appendix contains details about our approximate LDP solver and the whole MOT framework used in ApLift. We depict this framework in Figure 1.

**Appendix outline.** We start with providing additional notation and abbreviations list in Section 8.1. Sections 8.2-8.8 present the message passing solver implementation and the algorithms used for it. Sections 8.9-8.13.2 present details about processing of the tracking data. Finally, Section 8.14 discusses theoretical runtime of the solver and Section 8.15 presents examples of qualitative results. The Appendix is rather extensive, especially its algorithmic part. Therefore, we provide its section outline within the context of the whole method below.

**LDP solver outline.** Figure 2 contains a scheme of all algorithms used in our LDP solver. The algorithms are stated either in the main paper or in this Appendix. The solver performs an explicitly given number of message passing iterations. Section 8.7 describes the full solver run and an overview of all methods used within one message passing iteration. Once in five iterations, new primal solution is computed (Sections 4.6 and 8.8). Once in twenty iterations, new subproblems are separated and added to the problem. These are path and cut subproblems (see Sections 4.3 and 4.4). Methods for their separations are described in Sections 8.4 and 8.5.

**Message passing.** Messages are sent between the subproblems. Each subproblem creates messages to be sent by computing min-marginals of its variables. Section 8.2 presents algorithms used for obtaining min-marginals of inflow and outflow subproblems. The algorithms allow us to efficiently obtain min-marginals of all lifted or all base edges of a subproblem at once. Messages from cut and path

subproblems are obtained by modifications of the respective algorithms for their optimization. See Section 4.4 in the main text for the cut subproblem optimization and Section 8.3 for path subproblem optimization.

**Tightening by separation.** We create the new path and cut subproblems in order to tighten the LP relaxation of the problem (3). Section 8.6 discusses the guaranteed lower bound improvement achieved by separating the new subproblems using algorithms in Sections 8.4 and 8.5.

**Tracking.** The proposed tracking framework contains additional processing steps, which are briefly mentioned in the main paper. A detailed description and additional evaluation data is provided in this appendix. To construct the graph we calculate costs based on two features as described in Section 5.1 and add multiple scalings which details can be found in Section 8.9. We also determine very confident edges and set their cost based on heuristics explained in Section 8.12. Furthermore, additional implementation and training details for the classifier are presented in Sections 8.10 and 8.11. The efficient inference based on interval solutions is provided in Section 8.13.1. Finally we show details for the post-processing based on heuristics in Section 8.13.2.

### 8.1. Additional notation and abbreviations

- $x \in A^B$  denotes a mapping  $x : B \rightarrow A$ .
- $[n]$  denotes the set of numbers  $\{1, 2, \dots, n\}$ .
- LP: Linear programming.
- MP: Message passing.
- DP: disjoint paths problem.
- LDP: Lifted disjoint paths.
- DFS: Depth first search.
- MPLP: Max Product Linear Programming.

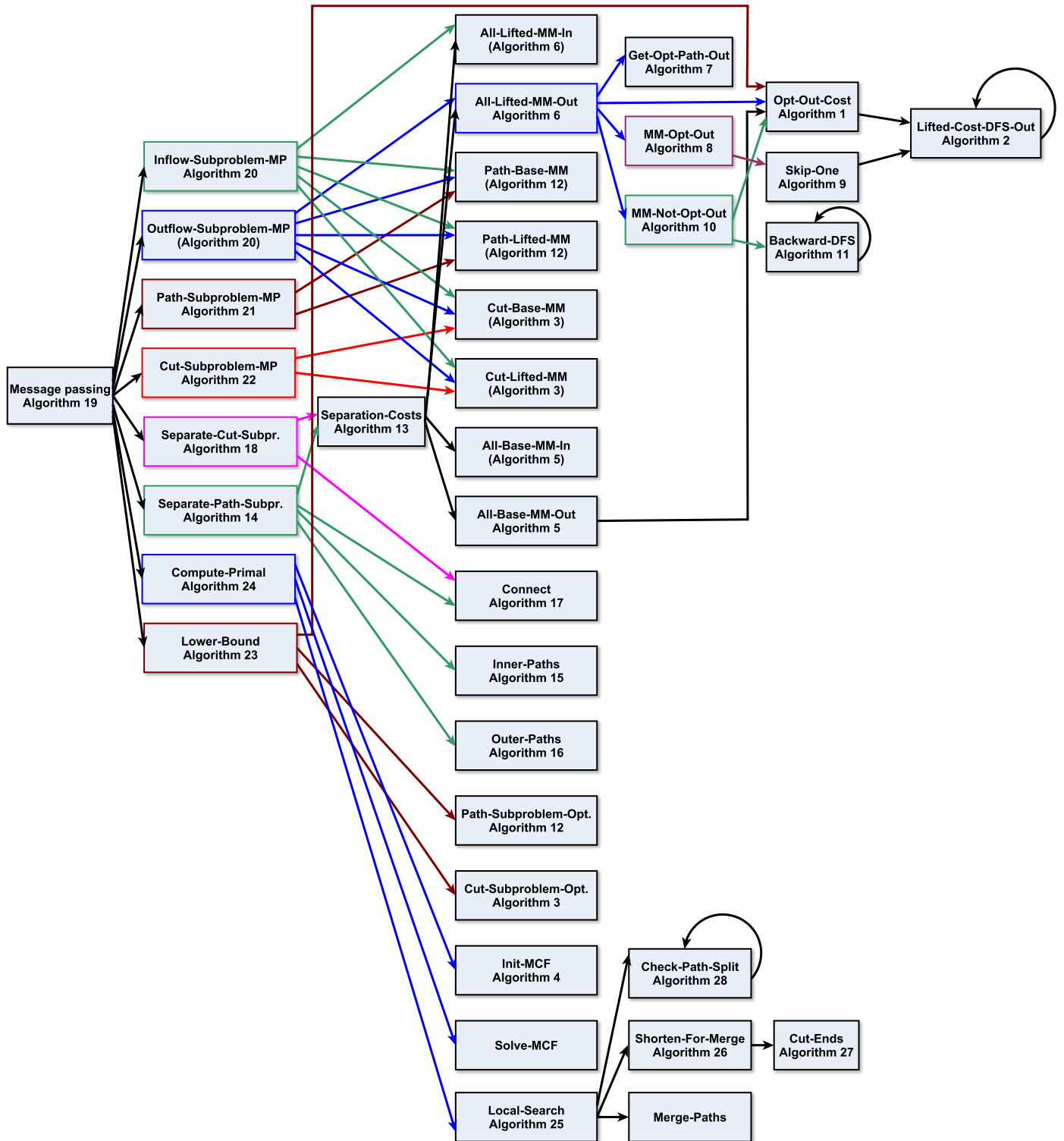


Figure 2. The scheme of our message passing algorithm and all its subroutines described in this work. An arrow from Algorithm  $X$  to Algorithm  $Y$  means that Algorithm  $X$  calls Algorithm  $Y$ . Algorithms in brackets denote that their modifications are used as the respective procedures. Abbreviation MP means Message-Passing. Some algorithms for inflow subproblems are omitted for clarity because they are analogous to outflow subproblem algorithms.

## 8.2. Min-Marginals for Inflow and Outflow Sub-problems

We detail routines for computing min-marginals for all base edges at once (Algorithm 5) and all lifted edges at once (Algorithm 6). All the stated algorithms assume outflow subproblems. Modification to inflow subproblems is done via proceeding in the opposite edge direction.

Iteratively computing min-marginals and performing operation (6) would be inefficient, since it would involve calling Algorithm 1  $\mathcal{O}(|\delta_E^+(v)| + |\delta_{E'}^+(v)|)$  times. To speed up iterative min-marginal updates, we can reuse computations as done in Algorithm 5 for base edges and in Algorithm 6 for lifted edges.

Algorithm 5 for computing base edge min-marginals uses the fact that lifted edge costs do not change and therefore Algorithm 1 needs to be called only once. For lifted edges, Algorithm 6 interleaves min-marginal computation and reparametrization updates (6) such that computations can be reused. We introduce auxiliary variables  $\gamma'_{vw}$  in line 3 that keep track of future reparametrization updates.

For the min-marginals, we will need slight extensions of Algorithm 1 and a method to additionally compute a labeling that attains the optimum. These methods are given in Algorithm 9 and 7.

In Algorithm 6, path  $P^*$  representing the optimal solution of the outflow problem is found by calling Algorithm 1 followed Algorithm 7. Then, Algorithm 8 computes min-marginals for the lifted edges that are active in the optimal solution. In the end of Algorithm 6, min-marginals are computed for those lifted edges that are not active in the optimal solution.

For computing min-marginals of edges that are active in the optimal solution, we need as a subroutine Algorithm 9, an extended version of Algorithm 1. Algorithm 9 restricts the vertices taken into consideration during the optimization. In particular, a special vertex  $r$  is given that is to be excluded from the optimization. Values  $\text{lifted\_cost}[u]$  are reused for those vertices  $u$  where  $ur \notin \mathcal{R}_G$  because these values are not affected by excluding vertex  $r$ .

Min-marginals for vertices inactive in the optimal solution are computed by Algorithms 10 and 11. The algorithms rely on structure  $\text{back\_cost}$  which is an analogy of  $\text{lifted\_cost}$ . Structure  $\text{back\_costs}[u]$  contains the minimum cost of all  $vu$ -paths w.r.t. to the costs of all lifted edges connecting  $v$  with the vertices of the path plus the cost of the first base edge of the path. Note that  $\text{lifted\_costs}[u]$  is defined analogically but contains the minimum cost of all  $ut$ -paths. Therefore, the minimal solution where a lifted edge  $vu \in E'$  is active can be obtained as follows:

$$\begin{aligned} \min_{(z,y,y') \in \mathcal{X}_v^{\text{out}}: y'_v=1} \langle (z_v, y, y'), \theta^{\text{out}} \rangle &= \\ &= \text{lifted\_cost}[u] + \text{back\_cost}[u] - \tilde{\theta}'_{vu} \quad (11) \end{aligned}$$

The cost of lifted edge  $\tilde{\theta}'_{vu}$  must be subtracted because it is involved in both values  $\text{lifted\_cost}[u]$  and  $\text{back\_cost}[u]$ .

Algorithm 11 performs two tasks simultaneously. First, it is a DFS procedure for computing  $\text{back\_cost}$ . Contrary to Algorithm 2 that performs DFS for obtaining  $\text{lifted\_cost}$ , Algorithm 11 proceeds in the opposite edge direction. It again uses the fact that a subpath of a minimum-cost path must be minimal. Second, it directly computes min marginal for already processed vertex  $u$  on Line 10 and involves this change in setting  $\text{back\_cost}[u]$  on Line 11.

**Speeding up DFS:** All the algorithms for obtaining optimal solution or min-marginals of inflow and outflow subproblems call DFS procedures. It can be considered that the order of processing the relevant nodes reachable from the central node is always the same. Therefore, we call DFS for each inflow and outflow subproblem only once during their initialization and store the obtained list of processed nodes. The full DFS in Algorithm 2 is replaced by traversing the precomputed node list in the forward direction. Algorithm 11 is replaced by traversing this node list in the backward direction.

---

### Algorithm 5 All-Base-MM-Out( $v, \tilde{\theta}$ )

---

**Input** start vertex  $v$ , costs  $\tilde{\theta}$

**Output** base edge min-marginals  $\gamma_{vu} \forall vu \in \delta_E^+(v)$

- 1:  $(\text{opt}, \text{lifted\_cost}, \alpha) = \text{Opt-Out-cost}(v, \theta^{\text{out}})$
  - 2:  $e^* = \underset{vw \in \gamma_E^+}{\text{argmin}} \{ \alpha_{vw} \}, e^{**} = \underset{vw \in \gamma_E^+ \setminus \{e^*\}}{\text{argmin}} \{ \alpha_{vw} \}$
  - 3:  $\forall vu \in \delta^+(v) : \gamma_{vu} = \alpha_{vu} - \min(\alpha_{e^{**}}, 0)$
- 

---

### Algorithm 6 All-Lifted-MM-Out( $v, \tilde{\theta}$ )

---

**Input** starting vertex  $v, \tilde{\theta}$

**Output** lifted edge min-marginals  $\gamma'_{vu} \forall vu \in \delta_{E'}^+(v)$

- 1:  $(\text{opt}, \text{lifted\_cost}, \alpha, \text{next}) = \text{Opt-Out-cost}(v, \theta^{\text{out}})$
  - 2:  $P_V^* = \text{Get-Opt-Path-Out}(\theta^{\text{out}}, \alpha, \text{next})$
  - 3:  $\forall vw \in \delta_{E'}^+(v) : \gamma'_{vw} = 0$
  - 4:  $(\text{opt}, \gamma') = \text{MM-Opt-Out}(v, P_V^*, \text{opt}, \gamma', \tilde{\theta})$
  - 5:  $\gamma' = \text{MM-Not-Opt-Out}(v, \text{opt}, \gamma', \tilde{\theta})$
-

---

**Algorithm 7** Get-Opt-Path-Out

---

**Input** costs  $\tilde{\theta}$ , vector  $\alpha$  such that  $\forall vw \in \delta_E^+(v) : \alpha_{vw}$  is the optimal value if  $vw$  is active, next

**Output** min cost path  $P_V^*$

```
1:  $w^* = \operatorname{argmin}_{w:vw \in \delta_E^+(v)} \alpha_{vw}$ 
2: if  $\alpha_{vw^*} < 0$  then
3:   while  $w^* \neq t$  do
4:      $P_V^* \leftarrow w^*$ 
5:      $w^* = \operatorname{next}[w^*]$ 
6:   end while
7: else
8:    $P_V^* = \emptyset$ 
9: end if
```

---

---

**Algorithm 8** MM-Opt-Out

---

**Input** starting vertex  $v$ , optimal path  $P_V^* = (v_1, \dots, v_k)$ , value of optimal path  $\operatorname{opt}$ ,  $\gamma'$ , costs  $\tilde{\theta}$

**Output** updated cost of optimal path  $\operatorname{opt}$ , new reparametrization updates  $\gamma'$

```
1: for all  $v_i = v_1, \dots, v_k : vv_i \in \delta_{E'}^+(v)$  do
2:    $\alpha = \operatorname{Skip-One}(v, v_i, \tilde{\theta} - (\mathbb{0}, \gamma'), \operatorname{lifted\_cost}, \operatorname{next})$ 
3:    $\gamma'_{vv_i} = \operatorname{opt} - \alpha$ 
4:    $\operatorname{opt} = \alpha$ 
5: end for
```

---

---

**Algorithm 9** Skip-One

---

**Input**  $v$ , ignored vertex  $r$ ,  $\tilde{\theta}$ ,  $\operatorname{lifted\_cost}$ , next

**Output** optimal value  $\operatorname{opt}$

```
1: for  $u \in V : vu \in \mathcal{R}_G \wedge ur \in \mathcal{R}_G$  do
2:    $\operatorname{lifted\_cost}[u] = \infty, \operatorname{next}[u] = \emptyset$ 
3: end for
4:  $\operatorname{lifted\_cost}[r] = 0, \operatorname{next}[r] = t$ 
5:  $\operatorname{Lifted-Cost-DFS-Out}(v, v, \tilde{\theta}, \operatorname{lifted\_cost}, \operatorname{next})$ 
6:  $\forall w : vw \in \delta_E^+(v) : \alpha_{vw} = \tilde{\theta}_v + \tilde{\theta}_{vw} + \operatorname{lifted\_cost}[w]$ 
7:  $\operatorname{opt} = \min(\min_{w:vw \in \delta_E^+(v)} \alpha_{vw}, 0)$ 
```

---

### 8.3. Optimization of path subproblems.

We denote by  $\theta^P$  the edge costs in subproblem of  $vw$ -path  $P$ . The optimization over the feasible set  $\mathcal{X}^P$  w.r.t. costs  $\theta^P$  is detailed in Algorithm 12. It checks whether there exists exactly one positive edge and whether it is either a lifted or a strong base edge (Line 2). If so, the optimal solution is either (i) all edges except the two largest ones (Line 6) or (ii) all edges (Line 8), whichever gives smaller objective value. If the above condition does not hold, the optimal solution can be chosen to contain all negative edges (Line 11).

A variation of Algorithm 12 with a specified edge fixed to either 0 or 1 is used for computing min-marginals

---

**Algorithm 10** MM-Not-Opt-Out

---

**Input**  $v$ , current optimum  $\operatorname{opt}$ , reparametrization update  $\gamma'$ ,  $\tilde{\theta}$

**Output** changed reparametrization update  $\gamma'$

```
1:  $(\operatorname{opt}, \operatorname{lifted\_cost}) = \operatorname{Opt-Out-cost}(v, \tilde{\theta} - (\mathbb{0}, \gamma'))$ 
2: for all  $u : vu \in \mathcal{R}_G$  do
3:   if  $u \in P_V^*$  then
4:      $\operatorname{visited}[u] = \operatorname{true}$ 
5:      $\operatorname{back\_cost}[u] = \operatorname{opt} - \operatorname{lifted\_cost}[u]$ 
6:     if  $vu \in E'$  then  $\operatorname{back\_cost}[u] += \theta'_{vu} - \gamma'_{vu}$ 
7:   else
8:      $\operatorname{visited}[u] = \operatorname{false}$ 
9:     if  $vu \in \delta_E^+(v)$  then
10:       $\operatorname{back\_cost}[u] = \tilde{\theta}_{vu}$ 
11:     else
12:       $\operatorname{back\_cost}[u] = \infty$ 
13:     end if
14:   end if
15: end for
16: for all  $vu \in \delta_{E'}^+(v)$  do
17:   if  $\operatorname{visited}[u] = \operatorname{false}$  then
18:      $\operatorname{Backward-DFS}(v, u, \tilde{\theta}, \gamma', \operatorname{opt}, \operatorname{back\_cost})$ 
19:   end if
20: end for
```

---

---

**Algorithm 11** Backward-DFS

---

**Input**  $v, u, \tilde{\theta}, \gamma', \operatorname{opt}, \operatorname{back\_cost}$

**Output**  $\gamma', \operatorname{back\_cost}$

```
1:  $\alpha = \operatorname{back\_cost}[u]$ 
2: for  $wu \in \delta_E^-(u) : vw \in \mathcal{R}_G$  do
3:   if  $\operatorname{visited}[w] = \operatorname{false}$  then
4:      $\operatorname{Backward-DFS}(v, w, \tilde{\theta}, \gamma', \operatorname{back\_cost})$ 
5:   end if
6:    $\alpha = \min\{\operatorname{back\_cost}[w], \alpha\}$ 
7: end for
8: if  $vu \in E'$  then
9:    $\operatorname{opt}_u = \alpha + \operatorname{lifted\_cost}[u]$ 
10:   $\gamma'_{vu} = \operatorname{opt}_u - \operatorname{opt}$ 
11:   $\operatorname{back\_cost}[u] = \alpha + \tilde{\theta}_{vu} - \gamma'_{vu}$ 
12: else
13:   $\operatorname{back\_cost}[u] = \alpha$ 
14: end if
15:  $\operatorname{visited}[u] = \operatorname{true}$ 
```

---

### 8.4. Separation for Path Subproblems

The path subproblem separation procedure is described in Algorithm 14. The algorithm finds paths together with a lifted edge connecting the start and the end point of the path such that exactly one lifted edge has positive cost, while all the remaining base and lifted edges have negative cost.

---

**Algorithm 12** Path-Subproblem-Optimization

---

**Input** Edge costs  $\theta^P$ **Output** optimal value  $\text{opt}$  of subproblem.

- 1:  $E^+ = \{kl \in P_{E'} \cup vw \mid \theta'_{kl} > 0\} \cup \{kl \in P_E \mid \theta_{kl} > 0\}$
  - 2: **if**  $E^+ = \{kl\} \wedge kl \in P_{E'} \cup vw \cup E_0$  **then**
  - 3:      $\alpha = \min\left\{\min_{ij \in P_E \setminus E^+} |\theta_{ij}^P|, \min_{ij \in P_{E'} \cup vw \setminus E^+} |\theta'_{ij}^P|\right\}$
  - 4:      $\beta = \begin{cases} \theta'_{kl}, & kl \in P_{E'} \cup vw \\ \theta_{kl}^P, & kl \in P_E \end{cases}$
  - 5:     **if**  $\alpha < \beta$  **then**
  - 6:          $\text{opt} = \sum_{ij \in P_E \setminus E^+} \theta_{ij}^P + \sum_{ij \in P_{E'} \cup vw \setminus E^+} \theta'_{ij}^P + \alpha$
  - 7:     **else**
  - 8:          $\text{opt} = \sum_{ij \in P_E} \theta_{ij}^P + \sum_{ij \in P_{E'} \cup vw} \theta'_{ij}^P$
  - 9:     **end if**
  - 10: **else**
  - 11:      $\text{opt} = \sum_{ij \in P_E \setminus E^+} \theta_{ij}^P + \sum_{ij \in P_{E'} \cup vw \setminus E^+} \theta'_{ij}^P$
  - 12: **end if**
  - 13: **return**  $\text{opt}$
- 

First, lifted and base edge costs are obtained in Algorithm 13 by computing min-marginals of inflow and outflow factors. Second, a graph with an empty edge set  $E^1$  is created. Then, edges with negative costs are added to  $E^1$  in ascending order. After adding an edge, we check whether separating path subproblems with edge costs leading to lower bound improvement is possible. Such a factor must contain the newly added edge, one positive lifted edge and edges that already are in the edge set  $E^1$ .

Algorithm 15 separates those paths subproblems where the only positive edge is the one connecting the path's endpoints. Algorithm 16 separates those path subproblems where the only positive edge is one of the edges within the path. Algorithm 17 updates connectivity structures by adding edge  $ij$  to the edge set  $E^1$ .

Each path subproblems has a guaranteed lower bound improvement, see Proposition 2. We add each found path subproblem to priority queue  $Q$ , where we sort w.r.t. the guaranteed lower bound improvement. After searching for path subproblems, we add the  $k$  best path subproblems from queue  $Q$  to the optimization problem.

### 8.5. Separation for Cut Subproblems

Algorithm 18 separates cut subproblems. The algorithm finds cuts consisting of base edges with positive costs and a lifted edge having endpoints on both sides of the cut and negative cost. Similarly as for the path subproblem separation, lifted and base edge costs are obtained by computing min-marginals of inflow and outflow factors in Algorithm 13. Each edge  $uv \in E'^-$  is a candidate lifted edge for a  $uv$ -cut factor.

---

**Algorithm 13** Separation-Costs

---

**Input** Current cost in inflow and outflow factors  $\theta^{in}, \theta^{out}$ **Output** Cost reparametrization  $\forall uv \in E : \tilde{\theta}_{uv}, \forall uv \in E' : \tilde{\theta}'_{uv}$ 

- 1:  $\forall uv \in E : \tilde{\theta}_{uv} = 0, \forall uv \in E' : \tilde{\theta}'_{uv} = 0$
  - 2: **for all**  $u \in V \setminus \{s, t\}$  **do**
  - 3:      $\forall uv \in \delta_E^+(u) : \gamma_{uv}^{out} = 0$
  - 4:      $\forall uv \in \delta_E^-(u) : \gamma_{vu}^{in} = 0$
  - 5:      $\gamma_u^{out} = 0.5 \cdot \text{All-Lifted-MM-Out}(u, \theta_u^{out})$
  - 6:      $\gamma_u^{in} = 0.5 \cdot \text{All-Lifted-MM-In}(u, \theta_u^{in})$
  - 7:      $\gamma_u^{out} = \text{All-Base-MM-Out}(u, \theta_u^{out} - (\gamma_u^{out}, \gamma_u^{out}))$
  - 8:      $\gamma_u^{in} = \text{All-Base-MM-In}(u, \theta_u^{in} - (\gamma_u^{in}, \gamma_u^{in}))$
  - 9:      $\forall uv \in \delta_E^+(u) : \tilde{\theta}_{uv} += \gamma_{uv}^{out}$
  - 10:      $\forall uv \in \delta_E^-(u) : \tilde{\theta}_{vu} += \gamma_{vu}^{in}$
  - 11:      $\forall uv \in \delta_{E'}^+(u) : \tilde{\theta}'_{uv} += \gamma_{uv}^{out}$
  - 12:      $\forall uv \in \delta_{E'}^-(u) : \tilde{\theta}'_{vu} += \gamma_{vu}^{in}$
  - 13: **end for**
- 

---

**Algorithm 14** Separate-Path-Subproblem

---

**Input** Cost threshold  $\varepsilon$ 

- 1:  $\tilde{\theta} = \text{Separation-Costs}(\theta^{in}, \theta^{out})$
  - 2:  $G^1 = (V, E^1 = \emptyset)$
  - 3:  $E^- = \{vw \in E \mid \tilde{\theta}_{vw} < -\varepsilon\} \cup \{vw \in E' \mid \tilde{\theta}'_{vw} < -\varepsilon\}$
  - 4:  $E'^+ = \{vw \in E' \mid \tilde{\theta}'_{vw} > \varepsilon\}$
  - 5:  $\forall v \in V : \text{desc}[v] = \{v\}, \text{pred}[v] = \{v\}$
  - 6: Priority-Queue  $Q = \emptyset$
  - 7: **for all**  $ij \in E^-$  ascending in  $\tilde{\theta}$  **do**
  - 8:     **if**  $ij \in E$  **then**  $c_{ij} = \theta_{ij}$
  - 9:     **else**  $c_{ij} = \theta'_{ij}$
  - 10:      $\text{Inner-Paths}(i, j, c_{ij}, \text{pred}, \text{desc}, E^+, E^1, Q)$
  - 11:      $\text{Outer-Paths}(i, j, c_{ij}, \text{pred}, \text{desc}, E^+, E^1, Q)$
  - 12:      $\text{Connect}(i, j, \text{pred}, \text{desc}, E^1)$
  - 13: **end for**
- 

---

**Algorithm 15** Inner-Paths

---

**Input**  $i, j, c_{ij}, \text{pred}, \text{desc}, E^+, E^1, Q$ 

- 1: **for all**  $p \in \text{pred}[i]$  **do**
  - 2:     **for all**  $d \in \text{desc}[j]$  **do**
  - 3:         **if**  $pd \in E^+$  **then**
  - 4:              $P_1 = \text{Find-Path}(p, i, E^1)$
  - 5:              $P_2 = \text{Find-Path}(j, d, E^1)$
  - 6:              $P = (P_1, ij, P_2)$
  - 7:              $\text{priority} = \min\{|c_{ij}|, \tilde{\theta}'_{pd}\}$
  - 8:              $Q \leftarrow (\text{Path-Problem}(P), \text{priority})$
  - 9:         **end if**
  - 10:     **end for**
  - 11: **end for**
- 

The edge set  $E^1$  initially contains all base edges with cost lower than  $\varepsilon$ . The remaining base edges are added to



---

**Algorithm 16** Outer-Paths

---

**Input**  $i, j, c_{ij}, \text{pred}, \text{desc}, E^+, E^1, Q$ 

```

1: for all  $p \in \text{pred}[j]$  do
2:   for all  $d \in \text{desc}[i]$  do
3:     if  $dp \in E^+$  then
4:        $P_1 = \text{Find-Path}(i, d, E^1)$ 
5:        $P_2 = \text{Find-Path}(p, j, E^1)$ 
6:        $P = (P_1, ij, P_2)$ 
7:        $\text{priority} = \min\{|c_{ij}|, \tilde{\theta}'_{dp}\}$ 
8:        $Q \leftarrow (\text{Path-Problem}(P), \text{priority})$ 
9:     end if
10:  end for
11: end for

```

---

**Algorithm 17** Connect

---

**Input**  $i, j, \text{pred}, \text{desc}, E^1$ 

```

1: for all  $p \in \text{pred}[i]$  do
2:   for all  $d \in \text{desc}[j]$  do
3:      $\text{desc}[p] \leftarrow d$ 
4:      $\text{pred}[d] \leftarrow p$ 
5:      $E^1 \leftarrow ij$ 
6:   end for
7: end for

```

---

$E^1$  in ascending order. Whenever a newly added edge  $ij$  causes a connection between  $u$  and  $v$  where  $uv \in E'^-$ , a  $uv$ -cut  $C$  is separated. We select the cut  $C$  to contain only those edges that do not belong to  $E^1$ . This ensures that  $ij$  is the weakest cut edge. In the same time,  $C$  is the best  $uv$ -cut with respect to the cost of the weakest cut edge.

The found cut factors are added to a priority queue where the priority represents guaranteed lower bound improvement (see Proposition 3) after adding the factor to our problem.

## 8.6. Tightening Lower Bound Improvement

In order to show that the separation procedures in Algorithms 14 and 18 lead to relaxations that improve the lower bound we show the following: (i) Certain reparametrization used in the above algorithms are non-decreasing in the lower bound. (ii) Separation procedures find new subproblems such that w.r.t. the above reparametrization, a guaranteed lower bound improvement can be achieved.

Points (i) and (ii) guarantee that the same lower bound achievement w.r.t. the original reparametrization can be found. The special reparametrization chosen helps empirically to find good subproblems.

**Lemma 1.** *Let  $s \in \mathcal{S}$  be a subproblem,  $\theta$  its cost and  $L_s(\theta)$  its lower bound for cost  $\theta$ . Given a cost reparametrization  $\gamma$  such that*

---

**Algorithm 18** Separate-Cut-Subproblem

---

**Input** Cost threshold  $\varepsilon$ 

```

1:  $\tilde{\theta} = \text{Separation-Costs}(\theta^{in}, \theta^{out})$ 
2:  $E'^- = \{vw \in E' | \tilde{\theta}'_{vw} < -\varepsilon\}$ 
3:  $E^- = \{vw \in E | \theta'_{vw} < \varepsilon\}, E^+ = E \setminus E^-$ 
4:  $E^1 = E^-, G^1 = (V, E^1)$ 
5: Priority-Queue  $Q = \emptyset$ 
6: for all  $ij \in E^+$  ascending in  $\tilde{\theta}$  do
7:   for all  $u \in \text{pred}[i]$  do
8:     for all  $v \in \text{desc}[j]$  do
9:       if  $uv \in E'^-$  then
10:         $C = \text{cut between } u, v \text{ using edges } E \setminus E^1$ 
11:         $\text{priority} = \min\{|\tilde{\theta}_{ij}|, |\tilde{\theta}'_{uv}|\}$ 
12:         $Q \leftarrow (\text{Cut-Problem}(C, u, v), \text{priority})$ 
13:      end if
14:    end for
15:  end for
16:   $\text{Connect}(i, j, \text{pred}, \text{desc}, E^1)$ 
17: end for

```

---

1.  $\forall i \in [d_s]$ 

$$\gamma_i = \begin{cases} \leq 0 & \text{if } \exists x^* \in \text{argmin}_{x \in \mathcal{X}^s} \langle \theta, x \rangle : x_i^* = 1 \\ \geq 0 & \text{if } \exists x^* \in \text{argmin}_{x \in \mathcal{X}^s} \langle \theta, x \rangle : x_i^* = 0 \end{cases} \quad (12)$$

2.  $\text{argmin}_{x \in \mathcal{X}^s} \langle \theta, x \rangle \subseteq \text{argmin}_{x \in \mathcal{X}^s} \langle \theta - \gamma, x \rangle$ 

and a coordinate-wise scaled reparametrization  $\gamma(\omega)$  defined by coefficients  $\omega \in [0, 1]^s$  where  $\forall i \in [d_s] : \gamma(\omega)_i = \omega_i \gamma_i$ , it holds:

1. The lower bound of  $s$  after reparametrization  $\gamma(\omega)$  is  $L_s(\theta - \gamma(\omega)) = L_s(\theta) - \sum_{i \in [d_s]: \gamma_i < 0} \omega_i \gamma_i$ .
2.  $\text{argmin}_{x \in \mathcal{X}^s} \langle \theta, x \rangle \subseteq \text{argmin}_{x \in \mathcal{X}^s} \langle \theta - \gamma(\omega), x \rangle$

*Proof.* We start with evaluating  $\langle \theta - \gamma(\omega), x^* \rangle$  where  $x^* \in \text{argmin}_{x \in \mathcal{X}^s} \langle \theta, x \rangle$ .

$$\begin{aligned} \langle \theta - \gamma(\omega), x^* \rangle &= \sum_{i \in [d_s]} (\theta_i - \omega_i \gamma_i) x_i^* = \\ &= \sum_{i \in [d_s]} \theta_i x_i^* - \sum_{i \in [d_s]: \gamma_i < 0} \omega_i \gamma_i x_i^* = \\ &= L_s(\theta) - \sum_{i \in [d_s]: \gamma_i < 0} \omega_i \gamma_i \end{aligned} \quad (13)$$

$\forall x \in \mathcal{X}, \forall x^* \in \operatorname{argmin}_{x \in \mathcal{X}^s} \langle \theta, x \rangle :$

$$\begin{aligned}
\langle \theta - \gamma(\omega), x \rangle &= \sum_{i \in [d_s]} (\theta_i - \omega_i \gamma_i) x_i = \\
&= \sum_{i \in [d_s]} (\theta_i - \gamma_i) x_i + \sum_{i \in [d_s]} (1 - \omega_i) \gamma_i x_i \geq \\
&\geq L_s(\theta - \gamma) + \sum_{i \in [d_s]: \gamma_i < 0} (1 - \omega_i) \gamma_i x_i = \\
&= \sum_{i \in [d_s]} (\theta_i - \gamma_i) x_i^* + \sum_{i \in [d_s]} (1 - \omega_i) \gamma_i x_i^* = \\
&= \langle \theta - \gamma(\omega), x^* \rangle
\end{aligned} \tag{14}$$

Formula 14 proves Point 2 of Lemma 1. Formulas 13 and 14 together prove Point 1.  $\square$

**Lemma 2.** Variables  $(\gamma_u^{\text{out}}, \gamma_u^{\prime \text{out}})$ , resp.  $(\gamma_u^{\text{in}}, \gamma_u^{\prime \text{in}})$  in Algorithm 13 satisfy the requirements of Lemma 1 for each outflow resp. inflow subproblem of vertex  $u$ .

*Proof.* Both Algorithms 5 and 6 output reparametrization variables that satisfy the requirements of Lemma 1. We have, for an outflow subproblem of node  $u$ :

$$\begin{aligned}
\operatorname{argmin}_{(y, y') \in \mathcal{X}_u^{\text{out}}} \langle \theta, (y, y') \rangle &\subseteq \operatorname{argmin}_{(y, y') \in \mathcal{X}_u^{\text{out}}} \langle \theta - (0, \gamma_u^{\text{out}}), (y, y') \rangle \\
&\subseteq \operatorname{argmin}_{(y, y') \in \mathcal{X}_u^{\text{out}}} \langle \theta - (\gamma_u^{\text{out}}, \gamma_u^{\prime \text{out}}), (y, y') \rangle
\end{aligned} \tag{15}$$

Therefore, also  $(\gamma_u^{\text{out}}, \gamma_u^{\prime \text{out}})$  together satisfy the requirements of Lemma 1. Analogically, for the inflow subproblems.  $\square$

**Costs in the new path and cut subproblems.** One edge is typically shared among multiple newly added path and cut subproblems. Therefore, the available cost reparametrizations  $\tilde{\theta}$  and  $\tilde{\theta}'$  from Algorithm 13 must be redistributed to the newly added subproblems. We denote the set of all newly added path subproblems resp. cut subproblems in tightening iteration  $i$  by  $\mathcal{P}^i$  resp.  $\mathcal{C}^i$ . For each base resp. lifted edge  $uv$ , we sum up the number of newly added path and cut subproblems that contain  $uv$ .

$$\begin{aligned}
N_{uv} &= |\{P \in \mathcal{P}^i : uv \in P_E\}| + |\{C \in \mathcal{C}^i : uv \in C_E\}|, \\
N'_{uv} &= |\{P \in \mathcal{P}^i : uv \in P_{E'}\}| + |\{P \in \mathcal{P}^i : P \text{ is a } uv\text{-path}\}| \\
&\quad + |\{C \in \mathcal{C}^i : C \text{ is a } uv\text{-cut}\}|.
\end{aligned} \tag{16}$$

Then, we define coefficient  $\omega_{uv}$  resp.  $\omega'_{uv}$  for each base edge  $uv \in E$  resp. lifted edge  $uv \in E'$  that belongs to a newly added subproblem as

$$\omega_{uv} = \frac{1}{N_{uv}}, \quad \omega'_{uv} = \frac{1}{N'_{uv}}. \tag{17}$$

Finally, for each newly added path subproblem  $P$  resp. cut subproblem  $C$ , we set the cost of base edge  $uv \in E$  to

$\theta_{uv}^P = \omega_{uv} \tilde{\theta}_{uv}$ , resp.  $\theta_{uv}^C = \omega_{uv} \tilde{\theta}_{uv}$ . Analogically, for the lifted edges.

**Cost update in in/outflow subproblems.** If we use an edge  $uv$  for creating one or more path and cut subproblems, it is necessary to update its cost in the inflow subproblem of vertex  $v$  and the outflow subproblem of vertex  $u$  accordingly. For instance, we update the cost of base edge  $uv$  in the outflow subproblem of  $u$  as follows  $\theta_{uv}^{\text{out}} \leftarrow \gamma_{uv}^{\text{out}}$ . Where we adopt the notation from Algorithm 13. Note that  $\tilde{\theta}_{uv} = \gamma_{uv}^{\text{in}} + \gamma_{uv}^{\text{out}}$ . Therefore, the total cost of edge variable  $uv$  is preserved.

**Proposition 2** (Guaranteed lower bound improvement of path subproblem). *If a path subproblem corresponding to  $vw$ -path  $P$  separated by Algorithm 14 is added to the subproblem set  $\mathcal{S}$ , the guaranteed improvement of the global lower bound is  $\min\{\min_{uv \in P_E} |\theta_{uv}^P|, \min_{uv \in P_{E'} \cup vw} |\theta_{uv}^P|\}$ , where  $\theta^P$  is the reparametrized cost used for the path factor initialization.*

*Proof.* Algorithm 14 separates only those subproblems that contain exactly one lifted edge with cost  $\theta_{uv}^P > \varepsilon$  and the rest of the edges have cost lower than  $-\varepsilon$ . The reparametrized costs of the path factor are fractions of cost reparametrizations obtained by Algorithm 13. We have

$$\begin{aligned}
\forall uv \in P_E : \\
\theta_{uv}^P &= \omega_{uv} \cdot (\gamma_{uv}^{\text{out}} + \gamma_{uv}^{\text{in}}), \\
\theta_{uv}^{\text{out}} &\leftarrow \omega_{uv} \cdot \gamma_{uv}^{\text{out}}, \quad \theta_{uv}^{\text{in}} \leftarrow \omega_{uv} \cdot \gamma_{uv}^{\text{in}}, \\
\forall uv \in P_{E'} : \\
\theta_{uv}^P &= \omega'_{uv} \cdot (\gamma_{uv}^{\text{out}} + \gamma_{uv}^{\text{in}}), \\
\theta_{uv}^{\text{out}} &\leftarrow \omega'_{uv} \cdot \gamma_{uv}^{\text{out}}, \quad \theta_{uv}^{\text{in}} \leftarrow \omega'_{uv} \cdot \gamma_{uv}^{\text{in}}
\end{aligned} \tag{18}$$

We evaluate the change of the lower bounds of all relevant inflow and outflow factors after reparametrization given by Formula 18. According to Lemma 1, we have

$$\begin{aligned}
\Delta L^{\text{out}} + \Delta L^{\text{in}} &= \\
&- \sum_{uv \in P_E: \gamma_{uv}^{\text{out}} < 0} \omega_{uv} \cdot \gamma_{uv}^{\text{out}} - \sum_{uv \in P_{E'} \cup vw: \gamma_{uv}^{\text{out}} < 0} \omega'_{uv} \cdot \gamma_{uv}^{\text{out}} \\
&- \sum_{uv \in P_E: \gamma_{uv}^{\text{in}} < 0} \omega_{uv} \cdot \gamma_{uv}^{\text{in}} - \sum_{uv \in P_{E'} \cup vw: \gamma_{uv}^{\text{in}} < 0} \omega'_{uv} \cdot \gamma_{uv}^{\text{in}} \geq \\
&- \sum_{uv \in P_E: \gamma_{uv}^{\text{out}} + \gamma_{uv}^{\text{in}} < 0} \omega_{uv} \cdot (\gamma_{uv}^{\text{out}} + \gamma_{uv}^{\text{in}}) - \\
&- \sum_{uv \in P_{E'} \cup vw: \gamma_{uv}^{\text{in}} + \gamma_{uv}^{\text{out}} < 0} \omega'_{uv} \cdot (\gamma_{uv}^{\text{out}} + \gamma_{uv}^{\text{in}}) = \\
&- \sum_{uv \in P_E: \theta_{uv}^P < 0} \omega_{uv} \cdot \theta_{uv}^P - \sum_{uv \in P_{E'} \cup vw: \theta_{uv}^P < 0} \omega'_{uv} \cdot \theta_{uv}^P
\end{aligned} \tag{19}$$

Let  $kl \in P_{E'}$  be the only lifted edge with positive cost in the path subproblem. We set  $\alpha =$

$\min\{\min_{ij \in P_E} |\theta_{ij}^P|, \min_{ij \in P_{E'} \cup vw \setminus kl} |\theta'_{ij}{}^P|\}$  as in Algorithm 12. If we denote by  $\Delta L^P$  the lower bound of the path subproblem, the global lower bound change after adding the path subproblem is:

$$\Delta L = \Delta L^{out} + \Delta L^{in} + \Delta L^P \quad (20)$$

If  $\alpha < \theta'_{kl}{}^P$

$$\begin{aligned} & \Delta L^{out} + \Delta L^{in} + \Delta L^P \geq \\ & - \sum_{uv \in P_E: \theta_{uv}^P < 0} \omega_{uv} \cdot \theta_{uv}^P - \sum_{uv \in P_{E'}: \theta'_{uv}{}^P < 0} \omega'_{uv} \cdot \theta'_{uv}{}^P + \\ & + \sum_{uv \in P_E: \theta_{uv}^P < 0} \omega_{uv} \cdot \theta_{uv}^P + \sum_{uv \in P_{E'}: \theta'_{uv}{}^P < 0} \omega'_{uv} \cdot \theta'_{uv}{}^P + \\ & + \alpha = \alpha \end{aligned} \quad (21)$$

If  $\alpha \geq \theta'_{kl}{}^P$

$$\begin{aligned} & \Delta L^{out} + \Delta L^{in} + \Delta L^P \geq \\ & - \sum_{uv \in P_E: \theta_{uv}^P < 0} \omega_{uv} \cdot \theta_{uv}^P - \sum_{uv \in P_{E'} \cup vw: \theta'_{uv}{}^P < 0} \omega'_{uv} \cdot \theta'_{uv}{}^P + \\ & + \sum_{uv \in P_E: \theta_{uv}^P < 0} \omega_{uv} \cdot \theta_{uv}^P + \sum_{uv \in P_{E'}: \theta'_{uv}{}^P < 0} \omega'_{uv} \cdot \theta'_{uv}{}^P = \\ & = \theta'_{kl}{}^P \end{aligned} \quad (22)$$

□

**Proposition 3** (Guaranteed lower bound improvement of cut subproblem). *If a subproblem corresponding to  $vw$ -cut  $C$  separated by Algorithm 18 is added to the subproblem set  $\mathcal{S}$ , the guaranteed improvement of the global lower bound is  $\min\{\min_{uv \in C} \theta_{uv}^C, |\theta'_{vw}{}^C|\}$ . Where  $\theta^C$  is the reparametrized cost used for the cut factor initialization.*

*Proof.* We obtain the reparametrized cost  $\theta^C$  for the cut subproblem analogically as in Formula 18 for the path subproblem. Note that Algorithm 18 ensures that all cut edges in the separated cut subproblem have positive cost and the lifted edge  $vw$  has negative cost. Using the same arguments as in the proof of Proposition 3, we obtain the lower bound change of inflow and outflow factors after separating the cut subproblem:

$$\begin{aligned} & \Delta L^{out} + \Delta L^{in} = \\ & - \sum_{uv \in C: \gamma_{uv}^{out} < 0} \omega_{uv} \cdot \gamma_{uv}^{out} - \sum_{uv \in C: \gamma_{uv}^{in} < 0} \omega'_{uv} \cdot \gamma_{uv}^{in} \\ & - \omega'_{vw} \gamma_{vw}^{out} - \omega'_{vw} \gamma_{vw}^{in} \geq \\ & - \sum_{uv \in C: \gamma_{uv}^{out} + \gamma_{uv}^{in} < 0} \omega_{uv} \cdot (\gamma_{uv}^{out} + \gamma_{uv}^{in}) - \omega'_{vw} \gamma_{vw}^{out} \\ & - \omega'_{vw} \gamma_{vw}^{in} = -\omega'_{vw} \gamma_{vw}^{out} - \omega'_{vw} \gamma_{vw}^{in} = -\theta'_{vw}{}^C \end{aligned} \quad (23)$$

Algorithm 3 shows how we obtain the lower bound of the cut subproblem. We set  $\theta_{ij}^C = \operatorname{argmin}_{uv \in C} \theta_{uv}^C$ . If  $\theta_{ij}^C < |\theta'_{vw}{}^C|$ , we get the overall lower bound improvement

$$\Delta L^{out} + \Delta L^{in} + \Delta L^C \geq -\theta'_{vw}{}^C + \theta'_{vw}{}^C + \theta_{ij}^C = \theta_{ij}^C.$$

If  $\theta_{ij}^C \geq |\theta'_{vw}{}^C|$ , the lower bound of the cut subproblem is 0 and the overall lower bound improvement is

$$\Delta L^{out} + \Delta L^{in} + \Delta L^C \geq -\theta'_{vw}{}^C. \quad (24)$$

□

## 8.7. Message Passing

One solver run consists of subproblems initialization and a number of message passing iterations. Algorithm 19 details the whole run. Algorithms 23-22 present methods that are called within one iteration.

The number of iterations is predetermined by an input parameter. We use typically tens or maximally one hundred iterations in our experiments.

Algorithm 19 sends in each iteration, messages between all subproblems in the subproblem set  $\mathcal{S}$ . Each subproblem creates messages to be sent by computing min-marginals of its variables (see Formula (5)). These min-marginals are re-scaled and redistributed between other subproblems that contain the respective variables. These operations are called reparametrization. See Section 4 for details.

Algorithm 23 computes lower bound of the LDP objective by summing up lower bounds of all subproblems. The cost reparametrization realized via our message passing procedures ensures that the lower bound is non-decreasing during the computation.

Algorithm 20 shows sending messages from the inflow subproblem of node  $u$ . Algorithm 21 shows sending messages from a path subproblem. Algorithm 22 presents sending messages from a cut subproblem.

---

**Algorithm 19** Message Passing

---

**Input** Graphs  $G = (V, E)$  and  $G' = (V, E')$ , costs  $\theta \in \mathbb{R}^{\bigcup_{E \cup E'} V}$

**Output** Best found primal solution  $(z, y, y')^{\text{ub}}$ , lower bound  $LB$

```
1: Initialization:
2: for  $v \in V$  do
3:   Add inflow subproblem for node  $v$ .
4:   
$$\forall uv \in \delta_{E'}^-(v) : \theta_{uv}^{in} = \begin{cases} \theta_{uv} & \text{if } v = s \\ \frac{1}{2}\theta_{uv} & \text{otherwise} \end{cases}$$

5:    $\forall uv \in \delta_{E'}^-(v) : \theta_{uv}'^{in} = \frac{1}{2}\theta_{uv}'$ .
6:    $\theta_v^{in} = \frac{1}{2}\theta_v$ .
7:   Add outflow subproblem for node  $v$  with analogous costs.
8: end for
9:  $\mathcal{C} = \emptyset$ 
10:  $\mathcal{P} = \emptyset$ 
11: Lagrange decomposition optimization
12: for  $\text{iter} = 1, \dots, \text{max\_iter}$  do
13:   Forward Pass:
14:   for  $u = u_1, \dots, u_{|V|}$  do
15:     Inflow-Subproblem-Message-Passing( $u$ )
16:     Outflow-Subproblem-Message-Passing( $u$ )
17:   end for
18:   for  $P \in \mathcal{P}$  do
19:     Path-Subproblem-Message-Passing( $P$ )
20:   end for
21:   for  $C \in \mathcal{C}$  do
22:     Cut-Subproblem-Message-Passing( $C$ )
23:   end for
24:   Backward Pass:
25:   Revert order of nodes and perform above iteration.
26:   if  $\text{iter} \equiv 0 \pmod k$  then
27:     Separate-Cut-Subproblem( $\varepsilon$ )
28:     Separate-Path-Subproblems( $\varepsilon$ )
29:     Add cut and path subproblems to  $\mathcal{C}$  and  $\mathcal{P}$ 
30:   end if
31:   if  $\text{iter} \equiv 0 \pmod l$  then
32:      $(z, y, y') = \text{Compute-Primal}(\mathcal{S}, \theta)$ 
33:     if  $\langle \theta, (z, y, y') \rangle < \langle \theta, (z, y, y')^{\text{ub}} \rangle$  then
34:        $(z, y, y')^{\text{ub}} = (z, y, y')$ 
35:     end if
36:   end if
37:    $LB = \text{Lower-Bound}$ 
38: end for
```

---

---

**Algorithm 20** Inflow-Subproblem-Message-Passing

---

**Input** central vertex  $u$  of the subproblem

```
1:  $\gamma^{in} = \text{All-Lifted-MM-In}(u, \theta^{in})$ .
2:  $\omega = 1$ 
3: for  $vu \in \delta_{E'}^-(u), P \in \mathcal{P} : vu \in P_E$  do
4:    $\gamma_{vu}^P = \text{Path-Base-Min-Marginal}(u, v, \theta^{in})$ 
5:    $\omega += 1$ 
6: end for
7: for  $vu \in \delta_{E'}^-(u), P \in \mathcal{P} : vu \in P_{E'}$  do
8:    $\gamma_{vu}'^P = \text{Path-Lifted-Min-Marginal}(u, v, \theta^{in})$ 
9:    $\omega += 1$ 
10: end for
11: for  $vu \in \delta_{E'}^-(u), P \in \mathcal{P} : P \in vu\text{-paths}(G)$  do
12:    $\gamma_{vu}''^P = \text{Path-Lifted-Min-Marginal}(u, v, \theta^{in})$ 
13:    $\omega += 1$ 
14: end for
15: for  $vu \in \delta_{E'}^-(u), C \in \mathcal{C} : vu \in C_E$  do
16:    $\gamma_{vu}^C = \text{Cut-Base-Min-Marginal}(u, v, \theta^{in})$ 
17:    $\omega += 1$ 
18: end for
19: for  $vu \in \delta_{E'}^-(u), C \in \mathcal{C} : C$  is a  $vu$ -Cut do
20:    $\gamma_{vu}''^C = \text{Cut-Lifted-Min-Marginal}(u, v, \theta^{in})$ 
21:    $\omega += 1$ 
22: end for
23: for  $vu \in \delta_{E'}^-(u)$  do
24:    $\theta_{vu}^{in} -= \frac{1}{\omega} \cdot \gamma_{vu}^{in}, \theta_{vu}^{out} += \frac{1}{\omega} \cdot \gamma_{vu}^{in}$ 
25: end for
26: for  $vu \in \delta_{E'}^-(u), P \in \mathcal{P} : vu \in P_E$  do
27:    $\theta_{vu}^{in} -= \frac{1}{\omega} \cdot \gamma_{vu}^P, \theta_{vu}^P += \frac{1}{\omega} \cdot \gamma_{vu}^P$ 
28: end for
29: for  $vu \in \delta_{E'}^-(u), P \in \mathcal{P} : vu \in P_{E'}$  do
30:    $\theta_{vu}^{in} -= \frac{1}{\omega} \cdot \gamma_{vu}'^P, \theta_{vu}'^P += \frac{1}{\omega} \cdot \gamma_{vu}'^P$ 
31: end for
32: for  $vu \in \delta_{E'}^-(u), P \in \mathcal{P} : P \in vu\text{-paths}(G)$  do
33:    $\theta_{vu}^{in} -= \frac{1}{\omega} \cdot \gamma_{vu}''^P, \theta_{vu}''^P += \frac{1}{\omega} \cdot \gamma_{vu}''^P$ 
34: end for
35: for  $vu \in \delta_{E'}^-(u), C \in \mathcal{C} : vu \in C_E$  do
36:    $\theta_{vu}^{in} -= \frac{1}{\omega} \cdot \gamma_{vu}^C, \theta_{vu}^C += \frac{1}{\omega} \cdot \gamma_{vu}^C$ 
37: end for
38: for  $vu \in \delta_{E'}^-(u), C \in \mathcal{C} : C$  is a  $vu$ -Cut do
39:    $\theta_{vu}^{in} -= \frac{1}{\omega} \cdot \gamma_{vu}''^C, \theta_{vu}''^C += \frac{1}{\omega} \cdot \gamma_{vu}''^C$ 
40: end for
```

---

---

**Algorithm 21** Path-Subproblem-Message-Passing

---

**Input:**  $uv$ -Path  $P \in \mathcal{P}$ 

- 1:  $\gamma^P = \text{Path-Min-Marginals}(P, \theta^P)$
  - 2:  $\omega^P = \frac{1}{2 \cdot |P_E| + 2 \cdot |P_{E'}|}$
  - 3: **for**  $kl \in P_E$  **do**
  - 4:    $\theta_{kl}^P \text{ --} = \gamma_{kl}^P$
  - 5:    $\theta_{kl}^{in} \text{ --} = \omega^P \cdot \gamma_{kl}^P, \quad \theta_{kl}^{out} \text{ --} = \omega^P \cdot \gamma_{kl}^P$
  - 6: **end for**
  - 7: **for**  $kl \in P_{E'}$  **do**
  - 8:    $\theta_{kl}^P \text{ --} = \gamma_{kl}^P$
  - 9:    $\theta_{kl}^{in} \text{ --} = \omega^P \cdot \gamma_{kl}^P, \quad \theta_{kl}^{out} \text{ --} = \omega^P \cdot \gamma_{kl}^P$
  - 10: **end for**
- 

---

**Algorithm 22** Cut-Subproblem-Message-Passing

---

**Input:**  $uv$ -Cut  $C \in \mathcal{C}$ 

- 1:  $\gamma^C = \text{Cut-Min-Marginals}(C, \theta^C)$
  - 2:  $\omega^C = \frac{1}{2 \cdot |C_E| + 2}$
  - 3: **for**  $kl \in C_E$  **do**
  - 4:    $\theta_{kl}^C \text{ --} = 2\omega^C \cdot \gamma_{kl}^C$
  - 5:    $\theta_{kl}^{in} \text{ +=} \omega^C \cdot \gamma_{kl}^C, \quad \theta_{kl}^{out} \text{ +=} \omega^C \cdot \gamma_{kl}^C$
  - 6: **end for**
  - 7:  $\theta_{uv}^C \text{ --} = 2\omega^C \cdot \gamma_{uv}^C$
  - 8:  $\theta_{uv}^{in} \text{ +=} \omega^C \cdot \gamma_{uv}^C, \quad \theta_{uv}^{out} \text{ +=} \omega^C \cdot \gamma_{uv}^C$
- 

---

**Algorithm 23** Lower-Bound

---

**Input** Subproblems  $\mathcal{S}$ **Output** Lower bound value  $LB$ 

- 1:  $LB = 0$
  - 2: **for**  $u \in V \setminus \{s, t\}$  **do**
  - 3:    $LB \text{ +=} \text{Opt-In-Cost}(u, \theta^{in})$
  - 4:    $LB \text{ +=} \text{Opt-Out-Cost}(u, \theta^{out})$
  - 5: **end for**
  - 6: **for**  $P \in \mathcal{P}$  **do**
  - 7:    $LB \text{ +=} \text{Path-Subproblem-Optimization}(P, \theta^P)$
  - 8: **end for**
  - 9: **for**  $C \in \mathcal{C}$  **do**
  - 10:    $LB \text{ +=} \text{Cut-Subproblem-Optimization}(C, \theta^C)$
  - 11: **end for**
- 

## 8.8. Primal Solution and Local Search

Algorithm 24 summarizes the whole procedure for obtaining a primal solution. As stated in Section 4.6, we obtain an initial primal solution by solving MCF problem.

Given a feasible solution of the LDP, Algorithm 25 improves it by splitting and merging paths. While we obtain the costs for MCF from base and lifted edges costs in inflow and outflow factors (Algorithm 4), the local search procedure uses original input costs of base and lifted edges.

Algorithm 28 finds candidate split point of each path and recursively splits the path if the split leads to decrease of the

objective function.

For each vertex of each path, function *split* evaluates the cost of splitting the path after the vertex:

$$\forall v_j \in P_V = (v_1, \dots, v_n) : \quad (25)$$
$$\text{split}(v_j, P) = - \sum_{\substack{k \leq j, l > j, \\ v_k v_l \in E'}} \theta'_{v_k v_l} - \theta_{v_j v_{j+1}} + \theta_{sv_{j+1}} + \theta_{v_j t}$$

The second step of the primal solution post-processing by Algorithm 25 is merging paths. Before the path merging itself, some candidate pairs of paths need to be shortened at their ends in order to enable their feasible merging.

Algorithm 26 identifies pairs of those paths whose merging should lead to objective improvement but that cannot be connected directly due to missing base edge between their endpoints. In order to identify the desired paths pairs, several functions are used.

Function  $l^+(P_1, P_2)$  resp  $l^-(P_1, P_2)$  is the sum of positive resp. negative lifted edges from path  $P_1$  to path  $P_2$ . Function  $l(P_1, P_2)$  sums all lifted edges from  $P_1$  to  $P_2$ .

$$\forall P_1, P_2 \in \mathcal{P}$$
$$l^+(P_1, P_2) = \sum_{uv \in E': u \in P_1, v \in P_2, \theta'_{uv} \geq 0} \theta'_{uv}$$
$$l^-(P_1, P_2) = \sum_{uv \in E': u \in P_1, v \in P_2, \theta'_{uv} < 0} \theta'_{uv} \quad (26)$$
$$l(P_1, P_2) = l^+(P_1, P_2) + l^-(P_1, P_2)$$

We use the above values in functions *merge* and *merge<sub>τ</sub>* that evaluate the gain of merging two paths. Threshold  $\tau \leq 1$  constrains the ratio between the positive and the negative part of lifted cost function  $l$  that is considered acceptable for merging two paths.

$$\forall P_1 = (v_1, \dots, v_n), P_2 = (u_1, \dots, u_m) \in \mathcal{P} \quad (27)$$
$$\text{merge}(P_1, P_2) = \begin{cases} \theta_{v_n u_1} + l(P_1, P_2) & \text{if } v_n u_1 \in E \\ \infty & \text{otherwise} \end{cases}$$

$$\forall P_1 = (v_1, \dots, v_n), P_2 = (u_1, \dots, u_m) \in \mathcal{P}$$
$$\text{merge}_\tau(P_1, P_2) = \begin{cases} \infty & \text{if } v_n u_1 \notin E \vee \\ & l^+(P_1, P_2) > \tau |l^-(P_1, P_2)| \\ \theta_{v_n u_1} + l(P_1, P_2) & \text{otherwise} \end{cases} \quad (28)$$

Algorithm 27 is applied on all paths pairs found by Algorithm 26. It inspects whether shortening of one or both paths leads to a feasible connection that ensures a desired objective improvement. It iteratively removes either the last vertex of the first path or the first vertex of the second path and checks if a connection is possible and how much it costs.

The last part of Algorithm 25 considers merging paths. We use formula  $merge_\tau(P_i, P_j) - out(P_i) - in(P_j)$  to evaluate whether merging two paths is beneficial. Here  $in(P_j)$  denotes input cost to the first vertex of  $P_j$  and  $out(P_i)$  denotes output cost from the last vertex of  $P_i$ . We state the full formula just for completeness. We set the input and the output costs to zeros in our experiments. Using  $merge_\tau$  ensures that we connect the paths only if the ratio between the positive lifted cost  $l^+$  and negative lifted cost  $l^-$  between the paths is below the acceptable threshold.

---

**Algorithm 24** Compute-Primal

**Input** Subproblems  $\mathcal{S}$ , original costs  $\theta \in \mathbb{R}^{|V'|+|E|+|E'|}$

**Output** Primal solution  $(z, y, y')$

- 1: Init-MCF
  - 2: Obtain primal solution of MCF  $y^{mcf} \in \{0, 1\}^{E^{mcf}}$
  - 3: Set  $(z, y)$  according to  $y^{mcf}$
  - 4:  $y' = \text{Adjust-Lifted-Solution}(z, y)$
  - 5:  $(z, y, y') = \text{Local-Search}(z, y, y')$
- 

---

**Algorithm 25** Local-Search

**Input** Input primal solution  $z, y, y'$

**Output** Improved primal solution  $z, y, y'$

- 1: Obtain set of disjoint paths  $\mathcal{P} = \{P_1, \dots, P_n\}$  from  $y$
- 2: **for all**  $P \in \mathcal{P}$  **do**
- 3:      $\mathcal{P} = \text{Check-Path-Split}(P_i, \mathcal{P})$
- 4: **end for**
- 5:  $\mathcal{P} = \text{Shorten-For-Merge}(\mathcal{P})$
- 6: **while true do**
- 7:

$$(P_1, P_2) = \underset{(P_i, P_j) \in \mathcal{P} \times \mathcal{P}}{\operatorname{argmin}} \quad merge_\tau(P_i, P_j) - out(P_i) - in(P_j)$$

- 8:     **if**  $merge_\tau(P_1, P_2) - out(P_1) - in(P_2) < 0$  **then**
  - 9:          $\mathcal{P} = \text{Merge-Paths}(P_1, P_2, \mathcal{P})$
  - 10:     **else**
  - 11:         **break**
  - 12:     **end if**
  - 13: **end while**
  - 14:  $(z, y, y') = \text{Set-From-Paths}(\mathcal{P})$
- 

---

**Algorithm 26** Shorten-For-Merge

**Input** Set of paths  $\mathcal{P}$

**Output** Updated set of paths  $\mathcal{P}$

- 1: **for all**  $P_1 = (v_1, \dots, v_n) \in \mathcal{P}$  **do**
  - 2:      $P = \underset{P_2=(u_1, \dots, u_m) \in \mathcal{P}: v_n u_1 \in E}{\operatorname{argmin}} \quad merge(P_1, P_2)$
  - 3:      $P' = \underset{P_2=(u_1, \dots, u_m) \in \mathcal{P}: v_n u_1 \notin E}{\operatorname{argmin}} \quad l(P_1, P_2)$
  - 4:     **if**  $l(P_1, P') < merge(P_1, P) \wedge l(P_1, P') < 0$  **then**
  - 5:          $P^* = P', c = l(P_1, P')$
  - 6:     **else**
  - 7:          $P^* = P, c = merge(P_1, P)$
  - 8:     **end if**
  - 9:     **if**  $\text{pred}[P^*] = \emptyset \vee \text{score}[P^*] > c$  **then**
  - 10:          $\text{pred}[P^*] = P_1, \text{score}[P^*] = c$
  - 11:     **end if**
  - 12: **end for**
  - 13: **for all**  $P_2 = (u_1, \dots, u_m) \in \mathcal{P}$  **do**
  - 14:     **if**  $\text{pred}[P_2] = P_1 = (v_1, \dots, v_n) \wedge v_n u_1 \notin E$  **then**
  - 15:          $\mathcal{P} = \text{Cut-Ends}(P_1, P_2, \mathcal{P})$
  - 16:     **end if**
  - 17: **end for**
- 

---

**Algorithm 28** Check-Path-Split

**Input** Input path  $P$ , set of all paths  $\mathcal{P}$

**Output** Set of paths  $\mathcal{P}$

- 1:  $v_m = \operatorname{argmax}_{v_j \in P_V} \text{split}(v_j, P)$
  - 2: **if**  $\text{split}(v_m, P) < 0$  **then**
  - 3:      $(P_1, P_2) = \text{Split-Path}(P, v_m)$
  - 4:      $\mathcal{P}.\text{remove}(P), \mathcal{P}.\text{insert}(P_1), \mathcal{P}.\text{insert}(P_2)$
  - 5:      $\mathcal{P} = \text{Check-Path-Split}(P_1, \mathcal{P})$
  - 6:      $\mathcal{P} = \text{Check-Path-Split}(P_2, \mathcal{P})$
  - 7: **end if**
  - 8: **return**  $\mathcal{P}$
-

---

**Algorithm 27** Cut-Ends

---

**Input**  $P_1 = (v_1, \dots, v_m), P_2 = (u_1, \dots, u_m), \mathcal{P}, i_{max}$ **Output** New set of paths  $\mathcal{P}$ 

```
1:  $c_1 = \infty, c_2 = \infty$ 
2: while  $i_1 + i_2 < i_{max}$  do
3:    $P'_1 = (v_1, \dots, v_{n-i_1}), P'_2 = (u_{1+i_2}, \dots, u_m)$ 
4:    $P''_1 = (v_1, \dots, v_{n-i_1-1}), P''_2 = (u_{2+i_2}, \dots, u_m)$ 
5:   if  $merge(P'_1, P'_2) + merge(P''_1, P''_2) < \infty$  then
6:      $\alpha_1 = merge(P'_1, P'_2) + split(P_1, v_{n-i_1}) +$ 
        $split(P_2, u_{1+i_2})$ 
7:      $\alpha_2 = merge(P''_1, P''_2) + split(P_1, v_{n-i_1-1}) +$ 
        $split(P_2, u_{i_2})$ 
8:     if  $\alpha_1 < \alpha_2$  then  $c_1 = i_1 - 1, c_2 = i_2$ 
9:     else  $c_1 = i_1, c_2 = i_2 - 1$ 
10:    break
11:   else if  $merge(P'_1, P''_2) < \infty$  then
12:      $c_1 = i_1 - 1, c_2 = i_2$ 
13:    break
14:   else if  $merge(P''_1, P'_2) < \infty$  then
15:      $c_1 = i_1, c_2 = i_2 - 1$ 
16:    break
17:   else
18:      $\alpha_1 = l(P'_1, P''_2) + split(P_1, v_{n-i_1}) +$ 
        $split(P_2, u_{1+i_2})$ 
19:      $\alpha_2 = l(P''_1, P'_2) + split(P_1, v_{n-i_1-1}) +$ 
        $split(P_2, u_{i_2})$ 
20:     if  $\alpha_1 < \alpha_2$  then  $i_2 ++$ 
21:     else  $i_1 ++$ 
22:   end if
23: end while
24: if  $c_1 \neq \infty \wedge c_2 \neq \infty$  then
25:    $P'_1 = (v_1, \dots, v_{n-c_1}), P'_2 = (u_{1+c_2}, \dots, u_m)$ 
26:   if  $merge_\tau(P'_1, P'_2) < \infty$  then
27:     if  $c_1 > 0$  then
28:        $(P_{11}, P_{12}) = \text{Split-Path}(P_1, v_{n-c_1})$ 
29:        $\mathcal{P}.remove(P_1)$ 
30:        $\mathcal{P}.insert(P_{11}), \mathcal{P}.insert(P_{12})$ 
31:     end if
32:     if  $c_2 > 0$  then
33:        $(P_{21}, P_{22}) = \text{Split-Path}(P_2, u_{c_2})$ 
34:        $\mathcal{P}.remove(P_2)$ 
35:        $\mathcal{P}.insert(P_{21}), \mathcal{P}.insert(P_{22})$ 
36:     end if
37:   end if
38: end if
39: return  $\mathcal{P}$ 
```

---

## 8.9. Global Context Normalization

Our tracking system employs a global context normalization to obtain accurate features between detections (see Section 5.1). This section elaborates the implementation details.

Global context normalization puts similarity measurements into global perspective to form more meaningful feature values. For instance, global illumination changes will likely decrease measured appearance similarities between any pair of detections. Likewise, a scene where all people are far away from the camera will most likely result in less confident appearance similarity measurements. In both cases, positive matching pairs should have higher similarities than negative matching pairs but the absolute similarity values are reduced by the global effects. These and further effects make the interpretation of the similarity in absolute terms less meaningful. Global context normalization compensates such effects.

To this end, let  $\Omega_k = \{\sigma_{vw,k} : vw \in E\}$  comprise all computed similarity measurements for feature  $k \in \{\text{Spa}, \text{App}\}$  defined in Section 5.1. For each feature  $k$  and similarity measurement  $\sigma_{vw,k} \in \Omega_k$ , we define sets  $\text{GC}_{i,k}$  with  $i \in [5]$ . Each set  $\text{GC}_{i,k}$  induces two global context normalization features:  $\sigma_{vw,k} \cdot \max(\text{GC}_{i,k})^{-1}$  and  $\sigma_{vw,k}^2 \cdot \max(\text{GC}_{i,k})^{-1}$ .

The sets are defined w. r. t.  $\sigma_{vw,k} \in \Omega_k$  as follows:

$$\text{GC}_{1,k} = \{s_{vn,k} \in \Omega_k : n \in B\}. \quad (29)$$

$$\text{GC}_{2,k} = \{s_{mw,k} \in \Omega_k : m \in B\}. \quad (30)$$

$$\text{GC}_{3,k} = \{s_{vn,k} \in \Omega_k : n \in B \text{ and } f_n = f_w\}. \quad (31)$$

$$\text{GC}_{4,k} = \{s_{nw,k} \in \Omega_k : n \in B \text{ and } f_n = f_v\}. \quad (32)$$

$$\text{GC}_{5,k} = \{s_{mn,k} \in \Omega_k : m, n \in B\}. \quad (33)$$

where  $f_x$  denotes the frame of detection  $x$  and  $B$  the batch as defined in section 5.1. The sets  $\text{GC}_{1,k}$  and  $\text{GC}_{2,k}$  result in a normalization of the similarity score  $\sigma_{vw,k}$  over all outgoing or incoming edges to  $v$  or  $w$ , respectively. The set  $\text{GC}_{3,k}$  results in a normalization over all similarity scores for outgoing edges from  $v$  to a detection in frame  $f_w$ . Analogously, the set  $\text{GC}_{4,k}$  collects all edges from a detection of frame  $f_v$  to node  $w$ . Finally,  $\text{GC}_{5,k}$  normalizes the similarity score over all existing scores in the batch  $B$ .

## 8.10. Multi Layer Perceptron (MLP)

As reported in Section 5.1 we use a lightweight and scalable MLP to obtain edge costs. We use multiple instances of the same MLP structure. Each MLP is trained on edges that have a specific range of temporal gaps (more details in Section 5.1).

The MLP architecture is based on two fully connected (FC) layers. The input is a 22-dimensional vector (features with corresponding global context normalizations). LeakyReLU activation [43] is used for the first FC layer. The final layer (FC) has one neuron, whose output represents the cost value. For training, an additional sigmoid activation is added. The structure of the neural network is visualized in Figure 3.

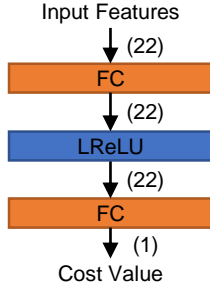


Figure 3. Visualisation of the proposed neural MLP. FC denotes fully connected layers, LReLU denotes LeakyReLU activation [43] and values in parenthesis denote the dimension of the corresponding tensors.

### 8.11. Batch Creation Using Fixed Frame Shifts

In this section, we elaborate on our batch creation method using fixed frame shifts (see Paragraph *Training* of Section 5.1).

A batch  $B$  contains a set of edges with corresponding edge costs. Important to note is that we use the same batch creation strategy to form batches for training as well as inference. During training, batches are augmented with corresponding ground truth labels. A carefully chosen batch creation strategy is crucial to ensure accurate and scalable training and inference.

In order to obtain accurate predictions by our MLPs (Section 5.1), the distribution of a batch should represent the characteristics of the training data. In particular, a batch should comprise edges covering all permissible temporal gaps between detections. Furthermore, the distribution of a batch influences the costs of all edges contained in the batch by the global context normalization (Section 8.9). Thus also during inference, a batch should comprise edges covering all permissible temporal gaps between detections. It is thus important to employ the same batch creation strategy for training and inference.

A naïve strategy is thus to define a batch on all frames within a range  $f$  up to  $f + \Delta f_{\max}$ , where  $f$  is a starting frame and  $\Delta f_{\max}$  defines the maximal permissible time gap. During training, one could then sample detections from these frames and randomly create true positive and false positive edges. However, such an approach is not tractable during inference for long sequences with many detections and long time gaps. To see this, consider the sequence MOT20-05 of the MOT20 dataset [16]. It contains 3315 frames with 226 detections per frame on average. We use a maximal permissible time gap of 2 seconds, which correspond to 50 frames for sequence MOT20-05. The number of edges per batch

and for the entire sequence can then be roughly estimated<sup>4</sup> with  $63 \cdot 10^6$  and  $4 \cdot 10^9$ , respectively, which is intractable.

To decrease the amount of edges per batch while ensuring that batches consists of samples containing all permissible temporal gaps, we adapt batch creation to our needs: For each start frame  $f$  of a batch, we subselect the frames to be considered within the range  $f, \dots, f_{\max}$ . During training, we then subsample detections from these frames. During inference, we utilize all detections of these frames to form our batch.

To this end, we define a sequence of frame shifts that is used to create the frame subselection. Using only few frame shift makes the approach more computationally efficient. Yet we must ensure that all edges are computed at least once during inference. That is if  $B(f)$  denotes the batch created according to our strategy with starting frame  $f$ , then  $\bigcup_f B(f) = E$  must contain all edges.

To ensure that we always cover temporal gaps of up to 2 seconds, the frame shifts depend on the maximal permissible temporal gaps (measured in frames).

For a start frame  $f$  and  $\Delta f_{\max} = 50$ , we define the frame shift set  $\text{Sh}(\Delta f_{\max})$  as

$$\text{Sh}(50) = \{0, 1, 2, 3, 4, 5, 6, 7, 8, 17, 26, 35, 44, 50\}. \quad (34)$$

For  $\Delta f_{\max} = 60$ , we define the frame shift set  $\text{Sh}(\Delta f_{\max})$  as

$$\text{Sh}(60) = \{0, 1, 2, 3, 4, 5, 6, 7, 14, 21, 28, 36, 37, 38, 40, 46, 53, 60\} \quad (35)$$

Then for each start frame  $f$ , a batch is created using the frames  $\{f + f_{\text{shift}} : f_{\text{shift}} \in \text{Sh}(f_{\max})\}$ . To ensure that all edges are computed at least once in the inference stage, one need to calculate batches with start frames  $f \in \{1 - \Delta f_{\max}, \dots, \Delta f_{\max}\}$ . Compared to the naïve batch creation strategy, our utilized batch creation results in  $226 \sum_{i=1}^{13} 226 \cdot (14 - i) = 4647916$  edges for MOT20-20, using the same assumptions as before. The number of edges to be computed is thus significantly lower.

### 8.12. Determining obviously matching and non-matching detection pairs

During the graph construction in Section 5.2, we employ a simply strategy to detect edges that represent obviously matching or obviously non-matching detection pairs. Corresponding edge costs are set such that they induce must-links or cannot-links as soft constraints. Details are described in this section.

**Obviously non-matching pairs.** We use optical flow and the object size to calculate the maximal plausible

<sup>4</sup>With 226 detections per frame, there are about  $226 \sum_{i=1}^{49} 226(50 - i) = 62568100$  edges per batch. With 3315 frames there are more than  $\frac{3315}{50} 62568100 = 4148265030$  edges. Here we assumed non-overlapping batches, thereby missing many connections.



displacement  $d_{\max}(v, w)$  and velocities  $v_{x,\max}(v, w)$  and  $v_{y,\max}(v, w)$  between two detections  $v$  and  $w$ . If  $v$  is a detection in frame  $f_v$  and  $w$  a detection in  $f_w$ , we define

$$d_{\max}(v, w) = k_d + \sum_{i=f_v}^{f_w-1} \max(O(i, i+1)) \quad (36)$$

where  $\max(O(i, i+1))$  is the maximal magnitude of the optical flow between the frames  $i$  and  $i+1$  and  $k_d$  is a security tolerance, which we set to 175 pixel according to experiments on the training data. If the distance  $d(v, w)$  between the center points of detections  $v$  and  $w$  is greater than  $d_{\max}(v, w)$ , the detection pair given by  $vw$  is regarded as obviously non-matching. We also assume that the maximal velocity of a person is limited. With the height  $h$  and width  $b$  of the bounding boxes, we define the maximal velocities

$$v_{x,\max}(v, w) = b \cdot k_e \quad (37)$$

and

$$v_{y,\max}(v, w) = h \cdot \frac{k_e}{2} \quad (38)$$

in  $x$  and  $y$ -direction. The factor  $k_e$  is set to  $k_e = 0.3$  according to experiments on the training data. In sequences with moving cameras, the factor is increased to  $k_e = 0.8$  and decreased to  $k_e = 0.12$  in sequences with static camera and aerial viewpoint. If the velocity  $v_x(v, w)$  or  $v_y(v, w)$  between the detections  $v$  and  $w$  is greater than corresponding  $v_{x,\max}(v, w)$  or  $v_{y,\max}(v, w)$ , the connection given by  $vw$  is regarded as obviously non-matching. To avoid wrong interpretations caused by noise in the velocity calculation, we set  $k_e$  to a high value for detection pairs with small temporal distances.

If a detection pair  $vw$  is regarded as obviously non-matching, we induce a cannot-link soft constraint on  $vw$  by setting its costs to a negative value with a high absolute value, *i.e.*  $c_{vw} \ll 0$ .

**Obviously matching pairs.** We induce must-link soft constraints on edges, considering only connections between consecutive frames.

An edge  $vw \in E$  with an appearance similarity score  $\sigma_{vw, \text{App}}$  close to the maximal achievable score (which is 2 in our implementation) is considered an obviously matching pair. We infer from the training data  $k_s = 1.95$  as threshold, so that edges with  $\sigma_{vw, \text{App}} > k_s$  are regarded as obviously matching by setting their costs accordingly.

In addition, if two boxes between consecutive frames have a high overlap, we induce a must-link soft constraint on the corresponding edge. In more detail, the intersection over union between the detections must be at least 0.5. However, such spatial measurements are affected by camera motions, thus potentially leading to wrong interpretations. In order to induce link soft-constraints only in confident cases, we employ a simple camera motion compensation beforehand. To this end, we calculate for a considered

Table 4. Results with and w/o post-processing on MOT20 train set.

	MOTA↑	IDF1↑	TP↑	FP↓	FN↓	IDS↓
w	<b>74.4</b>	62.8	<b>863203</b>	15778	<b>271411</b>	<b>3511</b>
w/o	72.3	<b>63.6</b>	833473	<b>8462</b>	301141	4201

edge the mean magnitude given by the optical flow between the frames of the respective detections. Before we compute the intersection over union, we translate one of the boxes in horizontal direction by the approximated camera motion, if this decreases the intersection over union. This procedure lowers the likelihood of creating wrong must-links caused by camera motion. Camera motion compensation needs to be applied only to sequences filmed from a non-static camera. Optical flow can be used to detect if a scene has a static camera setup. Note that MOT20 contains only scenes filmed from a static camera.

## 8.13. Inference

### 8.13.1 Interval Solution

This section explains how we solve MOT20 using solutions of its intervals. First, we solve the problem in independent subgraphs containing detections and edges from time intervals  $[il+1, (i+1)l]$  for  $i \in \{0, 1, \dots, n\}$ , where  $l = 3 \cdot t_{\max}$ , and  $t_{\max}$  is the maximum temporal edge length. We fix resulting trajectories in the centres of intervals, namely in time intervals  $[il+t_{\max}+1, (i+1)l-t_{\max}]$  for  $i \in \{1, \dots, n-1\}$ . Second, we solve the problem in time intervals covering the end of one initial interval and the beginning of the subsequent interval while allowing connections with the fixed trajectory fragments. The cost of a connection between a detection and a trajectory fragment is obtained as the sum of costs between the unassigned detection and the detections within the trajectory fragment.

### 8.13.2 Post-Processing

We perform post-processing on the result provided by our solver. As it is common, we recover missing detections within a computed trajectory using linear interpolation. We also correct wrong connections that mostly stem from situations which currently cannot be correctly resolved by current features, independent of the tracking system, *e.g.* pairwise features computed over very long temporal gaps and ambiguous feature information due to multiple people appearing within one detection box.

Consequently, we apply these strategies only to MOT20. As soon as one of these methods detects a connection as false, the corresponding trajectory is split into two new trajectories. Table 4 shows the effect of the post-processing on MOT20 train set.

We noticed an accumulation of wrong connections, where one end of a trajectory (*i.e.* its first or last detection) is connected to the successive detection using a skip-connection over a long temporal gap, and the connection is wrong. This might be explained by a combination of misleading visual features (*e.g.* caused by partial occlusion), not very informative spatial features (due to the high temporal gap) and missing lifted edges, because only one detection is existent at the end of the trajectory. To keep only reliable connections, we split trajectories if only one detection is existing at the start or end of a trajectory, followed by a temporal gap of at least 10 frames.

We also handle cases at the borders of a tracking scene. If a person leaves the scene, and another person enters the scene at a position close by after a short time, the tracking system sometimes joins the trajectories of the two persons. We explain this behaviour by the high visual similarity between partially visual persons at image borders. If a person leaves a scene, normally just one leg, one arm or the head is visible for some frames. However, a single body part is not very discriminative and thus can look similar to a body part of another person. In addition, the spatio-temporal information will indicate a likely match in this scenario. Due to the temporal gap, no or not many meaningful lifted edges are existing which could give contradicting signals. To eliminate this kind of errors, we split trajectories between two detections, if the temporal gap is greater or equal to 10 and both detections are located at the image border.

For all detections which are connected over a temporal time gap greater or equal to 10 frames (skip edges), we perform a motion sanity check and split the corresponding trajectory if its motion is not plausible. To this end, we first determine the highest velocity of obviously correct trajectories, or parts of trajectories with a minimal length of 10 frames (to avoid random noise issues). Then, we split connections at these skip edges, if their velocity is higher than the determined velocity.

Additionally, we verify that motion between trajectory parts are consistent. To this end, we consider the motion described by a trajectory, using the part before a connection, and compare it with the resulting motion described by the trajectory, using the part after the connection. If the velocities differ by a factor of 5 or greater or if the angle differs more than  $\pi/2$ , the trajectory is split.

## 8.14. Solver Runtime

Our solver can compute one interval of MOT20 (150 frames) or an entire sequence of MOT17 with less than 20GB RAM, using a single CPU core.

Subsequently, we analyze the runtime in detail, by performing a theoretical analysis in Section 8.14.1, followed by a comparison with an existing LDP solver in Section 8.14.2.

### 8.14.1 Computational Complexity

The solver terminates if one of the following conditions is satisfied. Either the lower bound is equal to the objective value of the best primal solution, *i.e.* optimum has been found. Or the maximum number of message passing iterations has been reached. The optimum was not found in our experiments, so the latter condition applied.

The runtime of the solver is, therefore, determined by the input parameter denoting the maximum number of iterations. The dependence on number of iterations is not exactly linear because the problem size grows with the number of path and cut subproblems added to set of subproblems  $S$  via cutting plane separation (see Sections 8.4 and 8.5).

An overview of the whole solver run and the tasks performed within one its iteration is given in Section 8.7. The runtime of the tasks is given by the runtime of computing min-marginals of the subproblems.

We discuss the complexity of the used algorithms in the paragraphs bellow. They all have a polynomial complexity. Therefore, the overall runtime of the solver is polynomial too.

In order to compute messages between the inflow and the outflow subproblem, we apply Algorithm 6. Min-marginals for messages between the path subproblems and the in/outflow subproblems are obtained for one shared variable at the time. The same holds for exchanging messages between the cut subproblems and the in/outflow subproblems. This is done by calling restricted versions of optimization algorithms of the path and cut subproblems (Algorithms 12 and 3). For in/outflow subproblems, we use one call of Algorithm 1 followed by either Algorithm 9 or Algorithm 11 limited to single variable reparametrization.

**Messages between inflow and outflow subproblems.** Messages between inflow and outflow subproblems are realized on lifted edge variables by calling Algorithm 6. Many subroutines employ full or partial DFS on all nodes reachable from the central node within the relevant time gap. In these cases, we use precomputed node order instead of complete DFS as described in the last paragraph of Section 8.2. One call of the full DFS (Algorithms 1 and 11) requires to process all vertices reachable from  $v$  within maximal time gap for edge length ( $\Delta f_{max}$ ). This comprises  $L_{max}$  video frames (we use  $L_{max} = 50$  or  $60$ ). Let us denote by  $n$  the maximum number of detections in one frame. The complete DFS processes maximally  $nL_{max}$  vertices. Incomplete DFS used in Algorithm 9 processes in each step vertices in  $L$  layers. In the worst case, this is done for all relevant layers  $L = 1, \dots, L_{max}$ . Processing one vertex requires to check its neighbors in the base graph. Their amount is bounded by  $KL_{max}$  where  $K = 3$ . See Sparsification paragraph in Section 5. Putting all together, the complexity of Algorithm 6 for one subproblem is  $\mathcal{O}(nL_{max}^3)$ . We have two subproblems for each (lifted)

graph vertex, yielding complexity  $\mathcal{O}(|V'|nL_{max}^3)$  for sending messages between all inflow and outflow subproblems in one message passing iteration.

**Messages from path subproblems.** Obtaining min marginal for one edge variable of a path subproblem requires two calls of restricted Algorithm 12 whose complexity is linear in the number of path edges. So, min-marginals for all path edges are obtained in  $\mathcal{O}(|P|^2)$ .

**Messages from cut subproblems.** Min marginal of one variable of a cut subproblems is obtained by adjusting its optimization Algorithm 3. The complexity is given by the complexity of the employed linear assignment problem which can be solved in polynomial time.

**Cutting plane procedures.** The cutting plane algorithms are called each 20 iterations. We allow to add maximally  $0.5 \cdot |\mathcal{S}_0|$  new factors during one separation call, where  $\mathcal{S}_0$  is the initial set of subproblems containing only inflow and outflow factors. So it holds,  $|\mathcal{S}_0| = 2|V'|$ . Once added, the subproblems influence the runtime via taking part in the message passing (see Section 8.7). Cutting plane itself (Sections 8.4 and 8.5) contains sorting of subsets of base or lifted edges which has complexity  $\mathcal{O}(|E^-| \log |E^-|)$  (resp.  $\mathcal{O}(|E^+| \log |E^+|)$ ). The other algorithms run in quadratic time w.r.t. number of vertices within relevant time distance to the currently processed edge.

**Primal solution.** We compute new primal solution in each five iterations. We use Algorithm 4 for obtaining base edge costs. Then, we use successive shortest paths algorithm for solving minimum cost flow problem and finally local search heuristic given by Algorithm 25, see Section 4.6. The complexity of solving MCF is the complexity of successive shortest path algorithm which is polynomial. Local search heuristic requires to compute and update cumulative costs between candidate paths. They can be computed in time linear in the number of lifted edges  $\mathcal{O}(|E'|)$ . MCF costs are obtained by calling Algorithm 1. Its complexity is discussed above.

### 8.14.2 Comparison with LifT

We perform several experiments for comparing our solver with an optimal solver for lifted disjoint paths LifT [28].

**LifT global solution vs. two-step procedure.** LifT is based on ILP solver Gurobi. It solves the LDP problem optimally. However, it is often not able to solve the problem on the full graphs. Therefore, LifT uses a two-step procedure. First, solutions are found on small time intervals to create tracklets. Second, the problem is solved on tracklets. This approach simplifies the problem significantly but the delivered solutions are not globally optimal anymore. We have observed that using our input costs, LifT is able to solve some problem sequences globally without the two step-procedure. Therefore, we compare our solver

with LifT using both the two-step procedure and the global solution.

**Influence of input costs.** Our input data contain many soft constraints for obviously matching pairs of detections. Those are edges with negative costs significantly higher in absolute value than other edges costs. LifT finds an initial feasible solution using only base edges. This solution may be already very good due to the costs of obviously matching pairs. Moreover, Gurobi contains a lot of efficient precomputing steps, so it can recognize that the respective variables should be active in the optimum and reduce the search space.

**Parameters.** We adjust parameters of our solver to work with comparable data as LifT. For instance, we do not set cost of any base edges to zero (as described in Section 5.2) because LifT does not enable this option. So, the costs of overlapping base and lifted edges are duplicated as opposed to the most of other experiments. Moreover, if there is no edge between two detections within the maximal time distance in the input data, we can add a lifted edge with high positive cost for such pair in ApLift. This is useful for reducing the input size for MOT20 dataset. LifT does not have this option. Therefore, we disable this option for ApLift too.

**Subsequences of MOT20.** We present a comparison between our solver and LifT using two-step procedure on an example subsequence of MOT20-01 in Table 3 in the main text. On that subsequence, our solver is faster and has even slightly better IDF1 score than LifT. In Table 5, we present a comparison on first  $n$  frames of sequence MOT20-02 where LifT finds solutions faster than our solver using many iterations. We assume that this is caused by the input costs that are convenient for Gurobi, see the discussion above.

**Train set of MOT17.** We compare our solver with LifT on global training sequences of MOT17. That is, we do not use two-step procedure. Therefore, LifT finds the globally optimal solution if it finishes successfully. The runtime of LifT is exponential in general and it can be often killed because of memory consumption if run on global sequences. Therefore, we perform these experiments on a machine having 2000 GB RAM and multiple CPUs each having 64 cores.

The results are in Table 6. Asterisk in LifT time column indicate that the problem cannot be finished. Some of the processes are killed by the system because of too much memory consumption. Some processes do not finish within more than 27 hours. Moreover, LifT often occupied up to 30 cores for solving one sequence. Our solver uses only one core. In the cases when LifT does not finish, we evaluate the best feasible solution found by LifT. Those were typically the initial feasible solutions. That is, the solutions that ignore the lifted edges. Obtaining the initial solutions for these difficult instances took between 1700 and 4600 seconds. The numbers in brackets relate our results to LifT

results. The time column provides the ratio between our time and LifT time. The IDF1 column presents the difference between ApLift and LifT.

Table 5. Runtime and IDF1 comparison of LDP solvers: ApLift (ours) with 6, 11, 31 and 51 iterations and LifT[28] (two step procedure) on first  $n$  frames of sequence *MOT20-01* from MOT20.

$n$	Measure	LifT	Our6	Our11	Our31	Our51
50	IDF1↑	<b>83.4</b>	<b>83.4</b>	<b>83.4</b>	<b>83.4</b>	<b>83.4</b>
	time [s]	62	4	7	25	46
100	IDF1↑	<b>80.6</b>	79.9	79.9	79.9	79.9
	time [s]	124	30	54	182	360
150	IDF1↑	<b>78.7</b>	76.8	76.8	76.8	76.8
	time [s]	222	61	110	378	780
200	IDF1↑	<b>77.6</b>	75.8	75.8	75.8	75.8
	time [s]	354	95	177	604	1195

### 8.15. Qualitative Results

Figure 4 and Figure 5 show qualitative tracking results from the MOT20 [16] and MOT17 [16] datasets. Comparing the samples, it becomes apparent that the density of objects in MOT20 is much higher than in MOT17. The sequence MOT20-04 (Figure 4) has an average density of 178.6 objects per frame and sequence MOT17-12 (Figure 5) only 9.6. The high density in MOT20 results in very crowded groups of persons which are occluding each other completely or partially. Accordingly, appearance information are ambiguous, leading to less discriminative edge costs. An additional challenge arises due to the distance between the camera and the persons, as well as global illumination changes in some sequences. The images shown in Figure 4 are captured in a temporal distance of 40 frames (*i.e.* 1.6 seconds) and the illumination changes heavily. This leads to appearance changes within a short time, which makes re-identification challenging. For instance, the person with id 666 (top right corner) in Figure 4 is wearing a red scarf and a beige jacket. Only a few frames later, the person is barely visible and colors have changed.

Despite these challenges, our system delivers accurate tracking results, as can be seen from the result images. Also the combinatorial and computational challenge in computing optimal trajectories for MOT20, considering for each detections all possible connections within a 50 frame range becomes apparent.

Result video for all test sequences can be obtain from the official evaluation server, for MOT15<sup>5</sup>, MOT16<sup>6</sup>, MOT17<sup>7</sup>, and MOT20<sup>8</sup>.

<sup>5</sup> <https://motchallenge.net/method/MOT=4031&chl=2>

<sup>6</sup> <https://motchallenge.net/method/MOT=4031&chl=5>

<sup>7</sup> <https://motchallenge.net/method/MOT=4031&chl=10>

<sup>8</sup> <https://motchallenge.net/method/MOT=4031&chl=13>

### 8.16. Tracking Metrics

A detailed evaluation of our proposed MOT system in terms of tracking metrics for all sequences of the datasets MOT20 [16] and MOT17 [45] are reported in Table 7. Evaluations on the test set are performed by the official benchmark evaluation server at <https://motchallenge.net> where our test results are reported as well. The tracking method for training sequences are trained with leave-one-out strategy to avoid overfitting on the corresponding training sequence.

Table 6. Runtime and IDF1 comparison of LDP solvers: ApLift (ours) with 6, 11, 31, 51 and 101 iterations and globally optimal (one step) Lift[28] on MOT17 train. Numbers in parenthesis in the time column show the difference between the solvers, in the IDF1 column the ratio between Lift and ApLift.

Sequence Name	Lift		Ours-6		Ours-11		Ours-31		Ours-51		Ours-101	
	Time↓	IDF1↑	Time↓	IDF1↑	Time↓	IDF1↑	Time↓	IDF1↑	Time↓	IDF1↑	Time↓	IDF1↑
02-DPM	7324 (1.0)	<b>49.4</b> (0.0)	94 (0.01)	47.4 (-2.00)	157 (0.02)	47.4 (-2.00)	513 (0.07)	49.1 (-0.30)	989 (0.14)	49.1 (-0.30)	2415 (0.33)	49.1 (-0.30)
02-FRCNN	4073 (1.0)	54.7 (0.0)	97 (0.02)	<b>54.9</b> (0.20)	161 (0.04)	<b>54.9</b> (0.20)	526 (0.13)	<b>54.9</b> (0.20)	1021 (0.25)	<b>54.9</b> (0.20)	2503 (0.61)	<b>54.9</b> (0.20)
02-SDP	7795 (1.0)	<b>56.7</b> (0.0)	131 (0.02)	55.0 (-1.70)	219 (0.03)	55.0 (-1.70)	717 (0.09)	55.0 (-1.70)	1410 (0.18)	55.0 (-1.70)	3685 (0.47)	55.0 (-1.70)
04-DPM	* (* )	<b>75.4</b> (0.0)	449 (* )	74.7 (-0.70)	756 (* )	74.7 (-0.70)	2220 (* )	74.7 (-0.70)	3929 (* )	75.0 (-0.40)	8578 (* )	75.0 (-0.40)
04-FRCNN	4889 (1.0)	<b>79.2</b> (0.0)	383 (0.08)	78.1 (-1.10)	644 (0.13)	78.1 (-1.10)	1811 (0.37)	76.3 (-2.90)	3111 (0.64)	78.2 (-1.00)	6565 (1.34)	78.2 (-1.00)
04-SDP	* (* )	<b>82.3</b> (0.0)	499 (* )	78.0 (-4.30)	839 (* )	78.0 (-4.30)	2441 (* )	78.0 (-4.30)	4294 (* )	77.7 (-4.60)	9269 (* )	79.9 (-2.40)
05-DPM	535 (1.0)	<b>65.0</b> (0.0)	10 (0.02)	62.6 (-2.40)	15 (0.03)	62.6 (-2.40)	57 (0.11)	63.5 (-1.50)	116 (0.22)	63.5 (-1.50)	298 (0.56)	63.5 (-1.50)
05-FRCNN	514 (1.0)	<b>66.6</b> (0.0)	10 (0.02)	63.8 (-2.80)	15 (0.03)	63.8 (-2.80)	57 (0.11)	64.0 (-2.60)	118 (0.23)	63.9 (-2.70)	315 (0.61)	65.6 (-1.00)
05-SDP	604 (1.0)	<b>67.9</b> (0.0)	11 (0.02)	<b>67.9</b> (0.00)	18 (0.03)	<b>67.9</b> (0.00)	67 (0.11)	67.1 (-0.80)	137 (0.23)	67.1 (-0.80)	364 (0.60)	67.6 (-0.30)
09-DPM	6692 (1.0)	<b>67.5</b> (0.0)	42 (0.01)	66.4 (-1.10)	70 (0.01)	66.4 (-1.10)	232 (0.03)	<b>67.5</b> (0.00)	480 (0.07)	<b>67.5</b> (0.00)	1281 (0.19)	<b>67.5</b> (0.00)
09-FRCNN	11888 (1.0)	<b>68.2</b> (0.0)	37 (0.00)	<b>68.2</b> (0.00)	61 (0.01)	<b>68.2</b> (0.00)	201 (0.02)	<b>68.2</b> (0.00)	407 (0.03)	<b>68.2</b> (0.00)	1095 (0.09)	<b>68.2</b> (0.00)
09-SDP	1462 (1.0)	<b>68.6</b> (0.0)	44 (0.03)	67.1 (-1.50)	74 (0.05)	67.1 (-1.50)	247 (0.17)	68.5 (-0.10)	512 (0.35)	68.5 (-0.10)	1443 (0.99)	68.5 (-0.10)
10-DPM	* (* )	66.0 (0.0)	279 (* )	<b>68.0</b> (2.00)	466 (* )	<b>68.0</b> (2.00)	1524 (* )	66.8 (0.80)	3087 (* )	67.0 (1.00)	9478 (* )	67.9 (1.90)
10-FRCNN	* (* )	65.2 (0.0)	310 (* )	68.8 (3.60)	511 (* )	68.5 (3.30)	1689 (* )	<b>69.4</b> (4.20)	3428 (* )	<b>69.4</b> (4.20)	10743 (* )	<b>69.4</b> (4.20)
10-SDP	* (* )	65.4 (0.0)	379 (* )	67.0 (1.60)	630 (* )	67.0 (1.60)	2090 (* )	67.4 (2.00)	4294 (* )	67.1 (1.70)	13379 (* )	<b>69.8</b> (4.40)
11-DPM	1991 (1.0)	<b>76.3</b> (0.0)	60 (0.03)	<b>76.3</b> (0.00)	99 (0.05)	<b>76.3</b> (0.00)	335 (0.17)	<b>76.3</b> (0.00)	672 (0.34)	<b>76.3</b> (0.00)	1672 (0.84)	<b>76.3</b> (0.00)
11-FRCNN	2382 (1.0)	<b>78.3</b> (0.0)	68 (0.03)	<b>78.3</b> (0.00)	113 (0.05)	<b>78.3</b> (0.00)	366 (0.15)	<b>78.3</b> (0.00)	729 (0.31)	<b>78.3</b> (0.00)	1799 (0.76)	<b>78.3</b> (0.00)
11-SDP	3195 (1.0)	80.0 (0.0)	68 (0.02)	79.8 (-0.20)	113 (0.04)	79.8 (-0.20)	370 (0.12)	<b>80.1</b> (0.10)	748 (0.23)	80.0 (0.00)	2057 (0.64)	80.0 (0.00)
13-DPM	* (* )	62.8 (0.0)	152 (* )	<b>66.8</b> (4.00)	252 (* )	<b>66.8</b> (4.00)	944 (* )	<b>66.8</b> (4.00)	2008 (* )	<b>66.8</b> (4.00)	6340 (* )	65.7 (2.90)
13-FRCNN	* (* )	62.5 (0.0)	217 (* )	<b>69.8</b> (7.30)	351 (* )	<b>69.8</b> (7.30)	1331 (* )	<b>69.8</b> (7.30)	2942 (* )	67.7 (5.20)	9813 (* )	66.2 (3.70)
13-SDP	* (* )	64.5 (0.0)	196 (* )	<b>66.8</b> (2.30)	326 (* )	<b>66.8</b> (2.30)	1237 (* )	<b>66.8</b> (2.30)	2698 (* )	66.2 (1.70)	8954 (* )	65.6 (1.10)
OVERALL	* (* )	<b>70.7</b> (0.0)	168 (* )	70.3 (-0.40)	280 (* )	70.3 (-0.40)	904 (* )	70.2 (-0.50)	1768 (* )	70.3 (-0.40)	4859 (* )	<b>70.7</b> (0.00)

Table 7. Evaluation results for training and test sequences for datasets MOT17 [45] and MOT20 [16]

Sequence		MOTA $\uparrow$	IDF1 $\uparrow$	MT $\uparrow$	ML $\downarrow$	FP $\downarrow$	FN $\downarrow$	IDS $\downarrow$	Frag. $\downarrow$
MOT20 Train	MOT20-01	65.8	62.0	31	10	180	6512	109	87
	MOT20-02	62.3	55.1	108	18	1393	56420	548	534
	MOT20-03	80.4	76.1	427	66	5427	55552	623	591
	MOT20-05	74.6	57.8	643	115	8778	152927	2231	2063
	OVERALL	74.4	62.8	1209	209	15778	271411	3511	3275
MOT20 Test	MOT20-04	79.3	68.8	412	40	8315	47364	968	840
	MOT20-06	36.1	36.8	41	111	4786	79313	740	744
	MOT20-07	56.9	54.7	40	15	936	13135	194	195
	MOT20-08	26.5	33.8	20	98	3702	52924	339	333
	OVERALL	58.9	56.5	513	264	17739	192736	2241	2112
MOT17 Train	MOT17-02-DPM	42.2	52.5	14	29	125	10588	26	26
	MOT17-02-FRCNN	47.3	58.4	15	21	227	9532	27	30
	MOT17-02-SDP	55.1	60.5	17	16	289	7994	53	52
	MOT17-04-DPM	70.9	78.9	40	21	340	13481	17	29
	MOT17-04-FRCNN	68.0	78.4	39	21	179	15044	5	13
	MOT17-04-SDP	77.9	80.8	47	13	439	10035	29	68
	MOT17-05-DPM	60.0	64.5	48	34	475	2260	31	24
	MOT17-05-FRCNN	57.8	64.0	55	32	650	2225	46	41
	MOT17-05-SDP	62.6	67.8	59	19	693	1842	53	46
	MOT17-09-DPM	73.0	72.8	14	1	46	1380	10	9
	MOT17-09-FRCNN	71.5	68.4	14	1	105	1403	10	9
	MOT17-09-SDP	74.1	72.9	14	1	66	1302	10	11
	MOT17-10-DPM	65.3	67.4	32	6	847	3545	61	74
	MOT17-10-FRCNN	62.8	65.8	40	2	2121	2513	139	114
	MOT17-10-SDP	66.3	66.5	43	2	1967	2189	173	120
	MOT17-11-DPM	69.2	75.7	34	21	248	2624	37	17
	MOT17-11-FRCNN	71.5	76.8	38	18	412	2233	47	15
	MOT17-11-SDP	72.6	78.5	42	13	547	1981	58	19
	MOT17-13-DPM	64.4	64.8	55	33	627	3436	83	56
	MOT17-13-FRCNN	67.8	63.4	77	8	1739	1892	120	76
MOT17-13-SDP	67.2	63.7	72	18	1388	2312	117	60	
OVERALL	66.0	71.4	809	330	13530	99811	1152	909	
MOT17 Test	MOT17-01-DPM	48.8	54.3	8	10	113	3181	8	21
	MOT17-01-FRCNN	47.0	57.5	9	10	360	3050	11	21
	MOT17-01-SDP	45.2	55.4	9	10	488	3033	13	29
	MOT17-03-DPM	73.8	73.4	85	17	4360	22905	118	261
	MOT17-03-FRCNN	72.8	74.7	74	17	3471	24883	109	234
	MOT17-03-SDP	77.7	75.4	94	13	4676	18482	139	386
	MOT17-06-DPM	57.7	61.2	94	76	1142	3765	77	91
	MOT17-06-FRCNN	57.3	58.4	102	59	1652	3279	102	140
	MOT17-06-SDP	57.2	59.5	107	58	1700	3251	87	125
	MOT17-07-DPM	45.7	52.5	11	15	1062	8038	80	126
	MOT17-07-FRCNN	45.0	53.1	11	15	1345	7862	75	135
	MOT17-07-SDP	46.6	53.8	13	11	1622	7310	87	166
	MOT17-08-DPM	33.7	44.3	17	37	421	13533	48	67
	MOT17-08-FRCNN	31.5	42.1	17	37	462	13948	53	74
	MOT17-08-SDP	34.5	45.2	18	34	445	13339	63	85
	MOT17-12-DPM	47.6	61.9	23	36	563	3959	20	32
	MOT17-12-FRCNN	47.8	62.3	18	40	296	4219	13	24
	MOT17-12-SDP	50.0	66.1	19	42	488	3836	11	31
	MOT17-14-DPM	37.8	51.0	19	71	1147	10191	151	150
	MOT17-14-FRCNN	33.9	48.4	25	62	2369	9636	206	228
	MOT17-14-SDP	37.0	49.9	25	58	2427	8970	238	246
	OVERALL	60.5	65.6	798	728	30609	190670	1709	2672



Figure 4. Example images from sequence MOT20-04 at frames 1092 and 1132. The images shows a crowded scene captured by a static camera. The above image is captured before an illumination change happens. The lower image is captured after an illumination change happens. The appearance of persons changes consequently to the illumination changes (e.g. ID 666 in the top right corner). The result video can be found at <https://motchallenge.net/method/MOT=4031&chl=13&vidSeq=MOT20-04>.

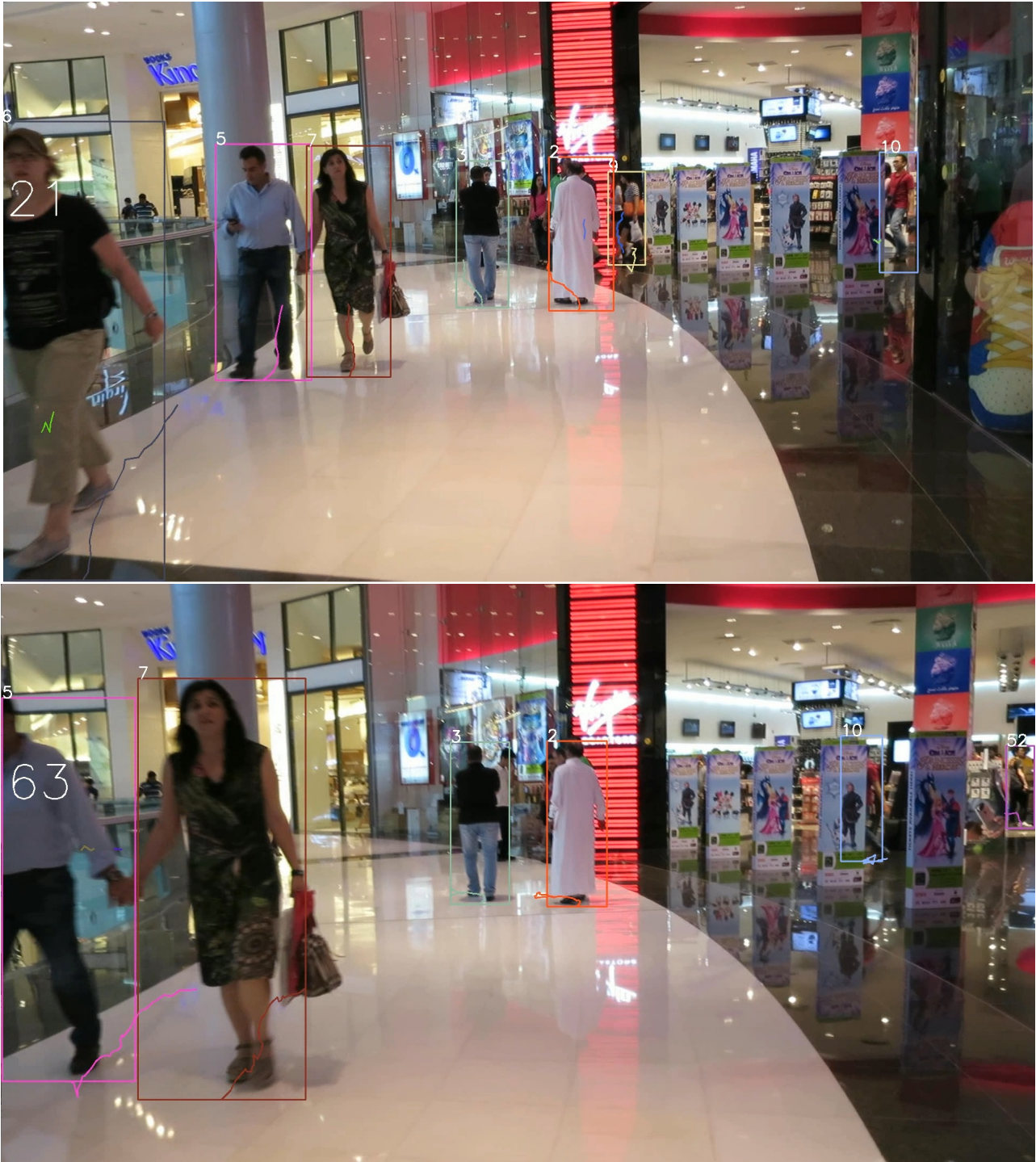


Figure 5. Example images from sequence MOT17-12 at frames 21 and 63. The image shows a scene captured by a moving camera. Compared to MOT20, the number of persons in the scene is lower and occlusions are seldom. The result video can be found at <https://motchallenge.net/method/MOT=4031&chl=10&vidSeq=MOT17-12-FRCNN>.